Computer-Aided Design 44 (2012) 1277–1296

Contents lists available at SciVerse ScienceDirect

Computer-Aided Design

journal homepage: www.elsevier.com/locate/cad

Constraint force design method for topology optimization of planar rigid-body mechanisms

Gil Ho Yoon *, Jae Chung Heo

School of Mechanical Engineering, Hanyang University, Republic of Korea

ARTICLE INFO

Article history:
Received 25 April 2011
Accepted 11 July 2012

Keywords:
Topology optimization
Rigid-body mechanism
Constraint force method

ABSTRACT

This study develops a new design method called the constraint force design method, which allows topology optimization for planar rigid-body mechanisms. In conventional mechanism synthesis methods, the kinematics of a mechanism are analytically derived and the positions and types of joints of a fixed configuration (hereafter the topology) are optimized to obtain an optimal rigid-body mechanism tracking the intended output trajectory. Therefore, in conventional methods, modification of the configuration or topology of joints and links is normally considered impossible. In order to circumvent the fixed topology limitation in optimally designing rigid-body mechanisms, we present the constraint force design method. This method distributes unit masses simulating revolute or prismatic joints depending on the number of assigned degrees of freedom, analyzes the kinetics of unit masses coupled with constraint forces, and designs the existence of these constraint forces to minimize the root-mean-square error of the output paths of synthesized linkages and a target linkage using a genetic algorithm. The applicability and limitations of the newly developed method are discussed in the context of its application to several rigid-body synthesis problems.

1. Introduction

This research presents a new mechanism synthesis method to determine the optimal configuration of links, i.e., the topology, including the joint type and optimal dimensions of rigid-link mechanisms. Ever since the concept of topology optimization (TO) was introduced, it has been applied to a large range of engineering problems and has recently become an important engineering tool [1–4]. Most recent and rigorous studies of TO focus on applications toward multiphysics problems as well as structural problems to optimize an objective that is subject to several constraints based on the finite element (FE) method. Among the many studies, TO of compliant and rigid mechanisms, as shown in Fig. 1, has also been actively researched by numerous scientists and engineers [1,4–19]. A number of studies have been carried out to discover the optimal topologies for compliant and rigid-body mechanisms by varying the material properties of the finite elements or the connectivity information of planar rigid-body mechanisms [5–19]. However, there are few TO methods that can provide mechanisms consisting of rigid links and joints as provided by conventional mechanism synthesis methods in the form of analytical formulations [18]. Therefore, to allow TO of rigid links for trajectory generation problems, we present a new TO method called the constraint force design method, which uses a genetic algorithm (GA) [20,21]. In [21], using the planar truss representation and the branch and bound method, the articulated mechanism is studied for path generation.

Most publications on dimensional syntheses dealing with path trajectory generation problems take an analytical approach using kinematics equations [22–27]. Typically, several precision positions on a target trajectory are first defined as reference points or target positions. Then, by changing the positions of the joints as well as the lengths of rigid links with a fixed topology, an optimal rigid-body linkage that minimizes the gap between the target positions and the current positions of a given design is pursued. Indeed, existing mechanism synthesis methods have limited workspace because of the fixed topologies of rigid-body links. Therefore, performance analyses of several fixed topologies appear to be essential. Furthermore, it is known that these mechanism synthesis approaches can possess what is known as prescribed timing conditions, which coordinate every position with a given value at the given time and input parameter (often an input angle or position).

To conduct the TO of rigid-body mechanisms dealing with the trajectory generation problem, in this study we present a new method called the constraint force design method, which

* Correspondence to: School of Mechanical Engineering, Hanyang University, Seoul, Republic of Korea. Tel.: +82 167875135.
E-mail addresses: gilho.yoon@gmail.com, ghy@hanyang.ac.kr (G.H. Yoon).

0010-4485/$ – see front matter © 2012 Elsevier Ltd. All rights reserved.
doi:10.1016/j.cad.2012.07.005

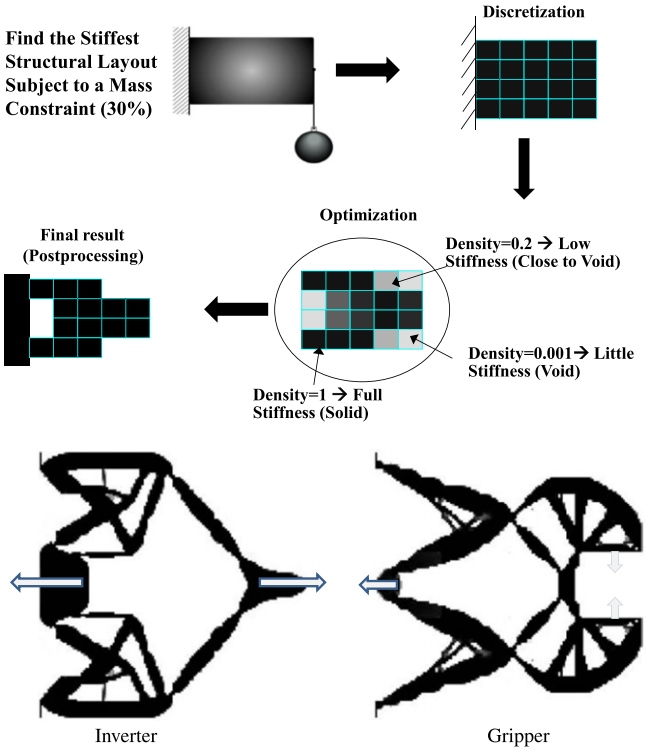

Fig. 1. Topology optimization and the design of a compliant mechanism [1,4].

parameterizes the existence of artificial forces satisfying the length constraints among masses with binary design variables, as shown in Fig. 2. With the newly developed approach, we expect to explore topologies satisfying given path trajectories. To implement this

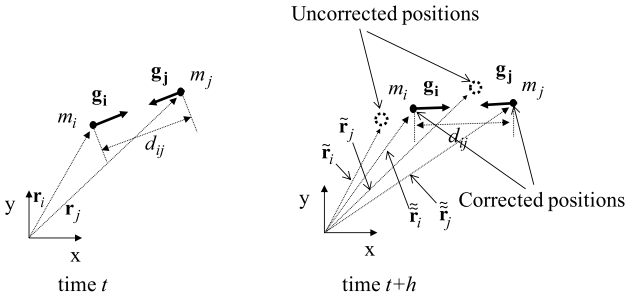

Fig. 4. Application of the length constraint method.

approach, we interpret unit masses as revolute or prismatic joints and the artificial forces acting on the unit masses to impose the relative lengths as rigid links. Unlike other mechanism synthesis approaches, we perform kinetic rather than kinematic analyses to analyze the positions of joints and links [28–34]. For the optimization formulation, we devise an objective function that minimizes the gap between the target trajectory and the current trajectory of a design as well as the number of rigid links. To tackle this optimization problem with many local optima effectively, the existence of the aforementioned artificial forces, which implies the existence of their corresponding links, is determined using a GA [20].

In this paper, after describing the analysis of rigid-body mechanisms using the Lagrangian formulation in Section 2, an optimization formulation using binary design variables is studied in Section 3. The employed GA is also described in Section 3. In Section 4, several numerical examples of rigid-body mechanism synthesis are presented to demonstrate the potential of the present approach. Finally, our findings and topics for future research are summarized and discussed.

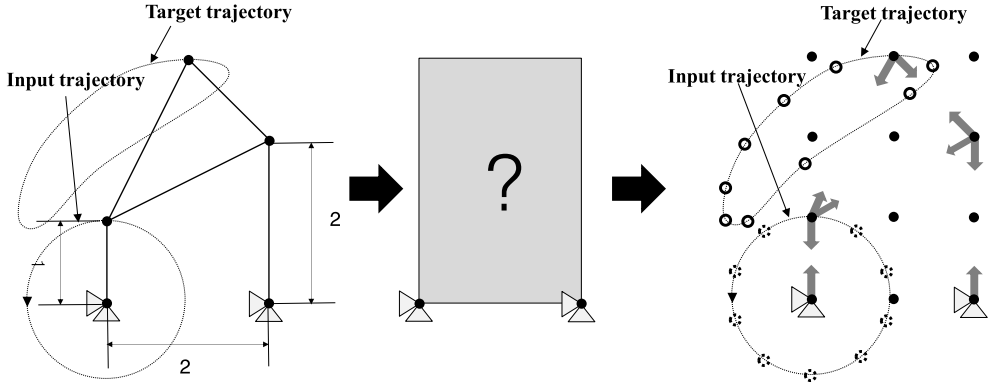

Fig. 2. Concept of the present TO for rigid-body mechanism design.

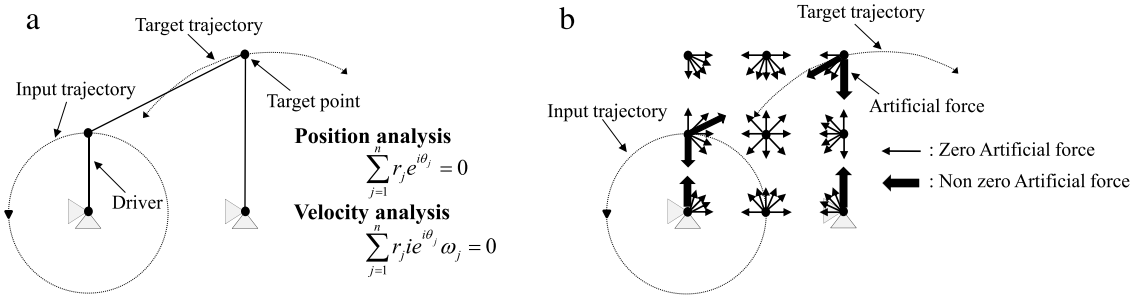

Fig. 3. Concept of the force constraint design method applied to a four-bar linkage. (a) Conventional analytical approach, and (b) the force constraint design method.

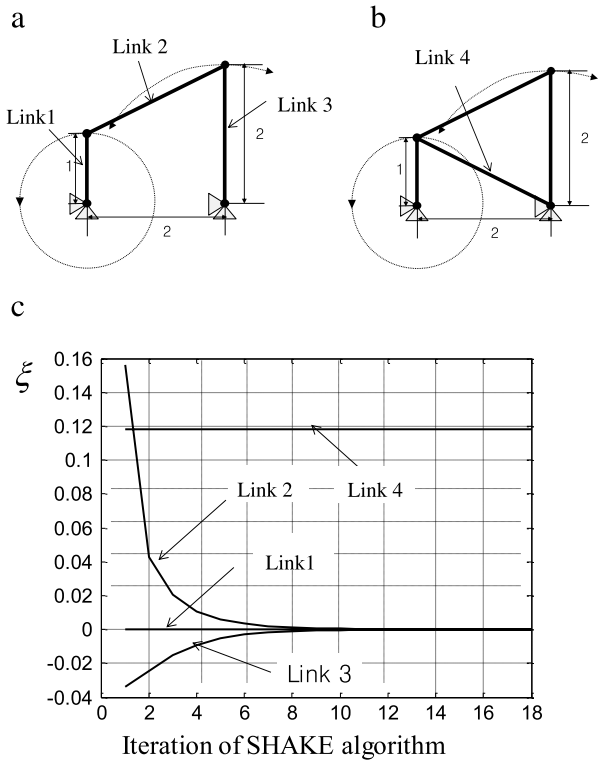

Fig. 5. Numerical examples of the SHAKE algorithm. (a) A four-bar mechanism, (b) a mechanism with no free degrees of freedom, and (c) the history of ξ in the SHAKE algorithm.

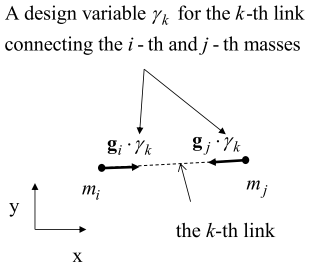

Fig. 7. Design parameterization of the existence of artificial constraint forces.

2. Rigid-body mechanism analysis using the Lagrangian formulation

2.1. Concept of the constraint force design method

Designing rigid-body mechanisms for various path trajectories has been an important and fundamental problem for many industrial applications such as for medical devices, transportation, and ordinary tool design [22–27]. Indeed, various mechanism synthesis methods for discovering optimal rigid-body mechanisms have been proposed. However, the majority of these methods are based on analytical and mathematical approaches that parameterize and optimize the dimensions of rigid links including the positions and types of joints; it is impossible to change configurations or topologies with these methods. From the perspective of optimization, these kinds of analytical and mathematical approaches can be considered size- and shape-optimization methods that are highly favorable for structural optimization with fixed topologies. Despite the vast amount of research on analytical approaches, studies exploring the optimal topologies of rigid-body mechanisms that give the closest trajectory to the target trajectory remain rare. In our opinion, if it were possible to discover optimal topologies for the target trajectory, it would be easy to satisfy complex output trajectories. To this end, in this study we newly develop the constraint force design method for optimizing the topology of planar rigid-body mechanisms. One of the distinct features of this method compared to existing mechanism synthesis methods is that kinetic analyses of a given mechanism are carried out instead of calculating kinematic information.

The key ideas of the present constraint force design method are that unit masses are represented as revolute or prismatic joints depending on displacement constraints, and that the artificial forces maintaining the relative lengths among the unit masses are represented as rigid links. To illustrate the basic concept, let us consider the trajectory simulation of the simplest four-bar mechanism in Fig. 3(a), whose trajectory can be obtained analytically. On the one hand, by rotating the driver (the left bar) with a certain angular speed, the trajectory of the target point is calculated by the guidance equation (kinematics) (Fig. 3(a)). On the other hand, to simulate this four-bar mechanism using the present approach, we first randomly distribute unit masses to simulate the

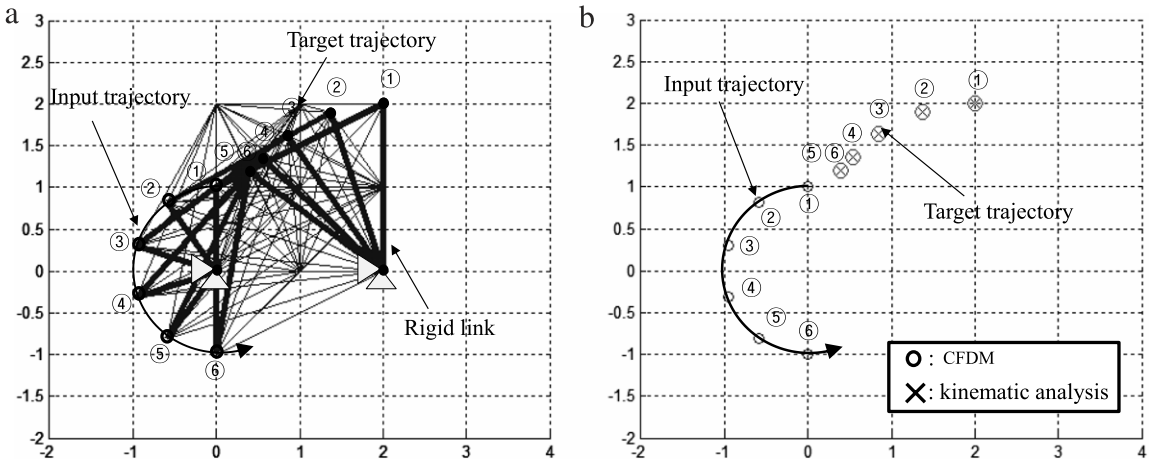

Fig. 6. A comparison between kinematic and kinetic analyses for the four-bar mechanism with $1, 2\sqrt{2}$ and 2 for its lengths. (a) The trajectory of kinetic analysis (the motions of the unit mass of the crank are equally constrained in order to impose the rotation of the crack) and (b) the comparisons of the trajectories between the kinetic analysis and the kinematics analysis.

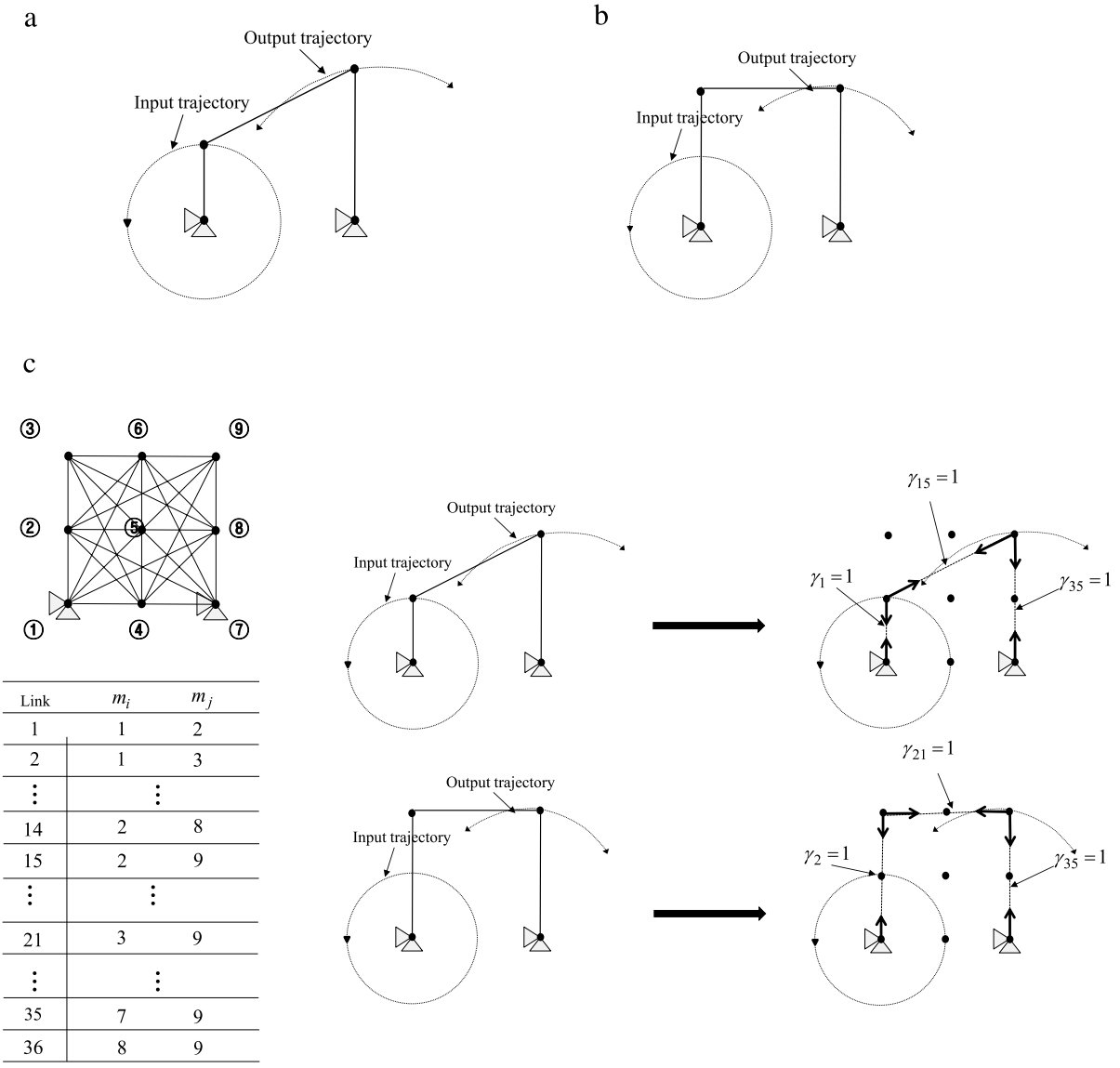

Link	m_i	m_j
1	1	2
2	1	3
⋮	⋮	
14	2	8
15	2	9
⋮	⋮	
21	3	9
⋮	⋮	
35	7	9
36	8	9

Fig. 8. Illustrative example of the present method for two four-bar mechanisms.

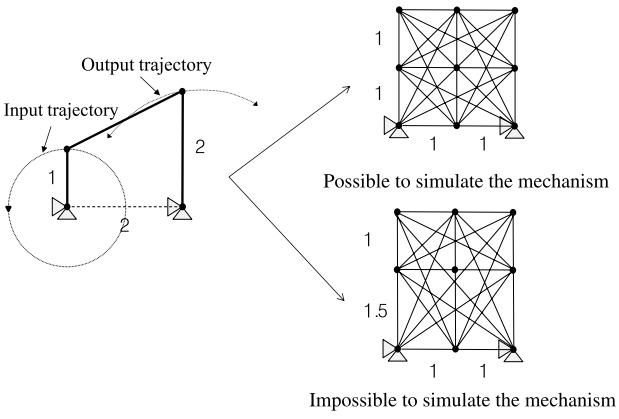

Fig. 9. Effect of initial mass distribution (a limitation of design space).

to-be-connected joints, as shown in Fig. 3(b). Here, nine masses are distributed to simulate revolute joints without any displacement or length constraints. Then, to mimic the four-bar mechanism of Fig. 3(a), length constraints are imposed among these nine masses during kinetic analysis. In other words, to simulate movements of the joints of the four-bar rigid link, the auxiliary forces maintaining the relative lengths, which are same as the actual lengths of the links, are imposed in the solution procedure of Newton's second law. Such analysis methods with artificial forces for relative length conditions are well established and many numerical methods have been developed [28–34]. Among them, the SHAKE algorithm based on the Lagrangian multiplier method is employed in this study. With this kinetic analysis including the auxiliary forces, the resulting trajectories of the masses are identical to the trajectories we seek to emulate.[1]

[1] The basic concept of the above-mentioned method is identical to that underlying the discrete element and molecular dynamics methods [29,30,34]. The differences among the methods lie in the fact that different potentials and associated forces are applied. However, the same principle and numerical codes can easily be transferred to from one method to another.

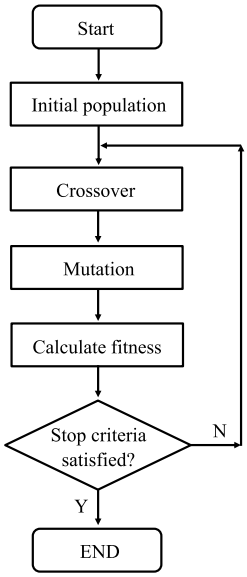

Fig. 10. General procedure of the genetic algorithm.

2.2. Basic principle of the Lagrangian formulation

Newton's second law.

The set of dynamic equations of masses with forces imposing the relative lengths among masses can be described by Newton's second law using the Lagrange equation as follows [34]:

$$\frac{d}{dt}\left(\frac{\partial L}{\partial \dot{\mathbf{r}}_i}\right) - \frac{\partial L}{\partial \mathbf{r}_i} = \sum_{k=1}^{N_i^{RL}} \lambda_k (\mathbf{r}_{ij}^2 - d_{ij}^2)$$

$$(i = 1, 2, 3, \ldots, n)\ (\mathbf{r}_{ij} = \mathbf{r}_i - \mathbf{r}_j,\ \mathbf{r}_{ij}^2 = \mathbf{r}_{ij} \cdot \mathbf{r}_{ij}) \tag{1}$$

$$L = \frac{1}{2}\sum_i m_i \dot{\mathbf{r}}_i^2 - U(\mathbf{r}_i) \quad (\mathbf{r}_i^2 = \mathbf{r}_i \cdot \mathbf{r}_i), \tag{2}$$

where L is the Lagrangian (the summation of kinetic energy and potential energy). The position and velocity of the i-th mass are denoted by $\mathbf{r}_i$ and $\dot{\mathbf{r}}_i$, respectively. The current distance vector and the imposed relative distance between the i-th and j-th masses are denoted by $\mathbf{r}_{ij}$ and d_{ij}, respectively; the second power of the length between the two masses is a scalar value $\mathbf{r}_{ij}^2$. The number of considered masses and the number of length constraints of the i-th mass are denoted by n and N_i^{RL}, respectively. Furthermore, it is assumed that each particle has a constant mass m. The Lagrangian multiplier for the k-th length constraint is denoted by λ_k in (1).

From the Lagrange equation above, the general equations regarding the motion of each mass are obtained as follows:

$$m_i \ddot{\mathbf{r}}_i = \mathbf{f}_i + \mathbf{g}_i \quad (i = 1, 2, 3, \ldots, n), \tag{3}$$

where the forces applied to the i-th mass independently of the other masses is denoted by $\mathbf{f}_i$, and the summed force acting on the i-th mass from the length constraints is denoted by $\mathbf{g}_i$ [28–34]. The acceleration vector of the i-th mass is denoted by $\ddot{\mathbf{r}}_i$.

To solve the above equations numerically, the well-established leap-frog method and the Verlet method are implemented. First, the position vector at time $t + h$ is expressed with the position vector at time t through Taylor expansion:

$$\tilde{\mathbf{r}}_i(t + h) = \mathbf{r}_i(t) + h\dot{\mathbf{r}}_i(t) + (h^2/2)\ddot{\mathbf{r}}_i(t) + O(h^3), \tag{4}$$

where the time integration step is denoted by h. The truncation error after the third expansion is denoted by $O(h^3)$. The velocity at time t can be approximated by the position vectors at $t + h$ and $t - h$.

$$\dot{\mathbf{r}}_i(t) = [\tilde{\mathbf{r}}_i(t + h) - \mathbf{r}_i(t - h)]/2h + O(h^2), \tag{5}$$

where the truncation error is denoted by $O(h^2)$. Note that in the employed approximation, the position vector at time $t + h$ is denoted by $\tilde{\mathbf{r}}_i$. Substituting (5) into (4) results in the following.

$$\tilde{\mathbf{r}}_i(t + h) = \mathbf{r}_i(t) + \frac{1}{2}\tilde{\mathbf{r}}_i(t + h) - \frac{1}{2}\mathbf{r}_i(t - h) + \frac{h^2}{2}\ddot{\mathbf{r}}_i(t), \tag{6a}$$

$$\frac{1}{2}\tilde{\mathbf{r}}_i(t + h) = \mathbf{r}_i(t) - \frac{1}{2}\mathbf{r}_i(t - h) + \frac{h^2}{2}\ddot{\mathbf{r}}_i(t), \tag{6b}$$

$$\tilde{\mathbf{r}}_i(t + h) = 2\mathbf{r}_i(t) - \mathbf{r}_i(t - h) + h^2\ddot{\mathbf{r}}_i(t). \tag{7}$$

Commonly, the higher-order error terms, i.e., $O(h^2)$ and $O(h^3)$, can be ignored and the position vector of the i-th mass can be written using (3) as follows:

$$\tilde{\mathbf{r}}_i(t + h) = 2\mathbf{r}_i(t) - \mathbf{r}_i(t - h) + \frac{h^2}{m}\mathbf{f}_i(t). \tag{8}$$

The above equation implies that it is possible to calculate the position of the i-th mass at time $t+h$ numerically using the location at time t and $t-h$ and the external force (or acceleration) at time t. In the derivations above, we do not consider the length constraints that simulate the constant lengths of rigid links. Indeed, we use the upper tilt for the uncorrected position to distinguish the updated position vector by (6) and (8) from the corrected position vector that considers the length constraint condition.

Length constraint method: the SHAKE algorithm.

As stated in the preceding sections, in order to impose the constant length condition among masses, the auxiliary force, $\mathbf{g}_i$, must be calculated and imposed upon each mass. To calculate these forces efficiently, the SHAKE algorithm is used. Through the imposition of the length conditions, we can modify the uncorrected position $\tilde{\mathbf{r}}_i$ with $\mathbf{g}_i$ (see [28–34] for more details). To explain the basic concept of this method and algorithm, let us consider the structure of Fig. 4.

We assume that the distance between the i-th and j-th masses at time t is d_{ij}. In addition, the positions of the two masses at time $t + h$ are calculated by (8). However, because the positions do not satisfy the length constraints, they must be corrected by considering the length constraint or applying the forces, $\mathbf{g}_i$, at time $t + h$, as shown in Fig. 4.

For the length constraint method, the current distance vector between the i-th and j-th masses is set to $\mathbf{r}_{ij} = \mathbf{r}_i - \mathbf{r}_j$ and the distance for the k-th rigid link is set to d_{ij} as follows:

$$\mathbf{r}_{ij}^2 = \left|\mathbf{r}_i - \mathbf{r}_j\right|^2 = d_{ij}^2 \quad \text{for the } k\text{-th rigid link.} \tag{9}$$

While solving Newton's second law to update the position of each mass, the length constraint described above should be properly imposed using the Lagrangian multiplier in (1). To impose this condition, we first define the scalar σ_k as follows:

$$\sigma_k \equiv \mathbf{r}_{i_k j_k}^2 - d_{i_k j_k}^2. \tag{10}$$

For the sake of clarity and convenience, the distance vector and the distance for the k-th rigid link are denoted by $\mathbf{r}_{i_k j_k}$ and $d_{i_k j_k}$, respectively; to our knowledge, these are common notations. The constraint force $\mathbf{g}_i$ in (3) can then be written as follows:

$$\mathbf{g}_i = -\sum_{k=C_i}^{N_i^{RL}} \lambda_k \nabla_i \sigma_k \quad \text{and} \quad (\nabla_i \sigma_k \equiv 2\mathbf{r}_{ij}), \tag{11}$$

where C_i is the set of the constraints directly involving $\mathbf{r}_i$. Eq. (8) can then be corrected as follows:

$$\mathbf{r}_i(t + h) = \tilde{\mathbf{r}}_i(t + h) - \frac{h^2}{m_i}\sum \lambda_k \nabla_i \sigma_k. \tag{12}$$

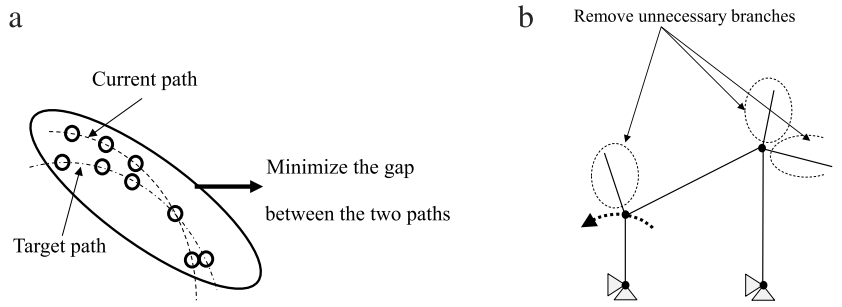

Fig. 11. Implications of the objective function (21). (a) Minimizing the gap between the two paths, and (b) removing unnecessary branches.

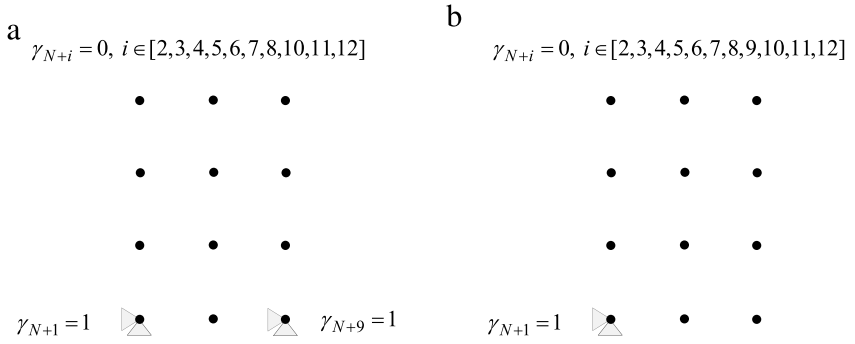

Fig. 12. Example of design variables for support with 12 masses ($N = 66$).

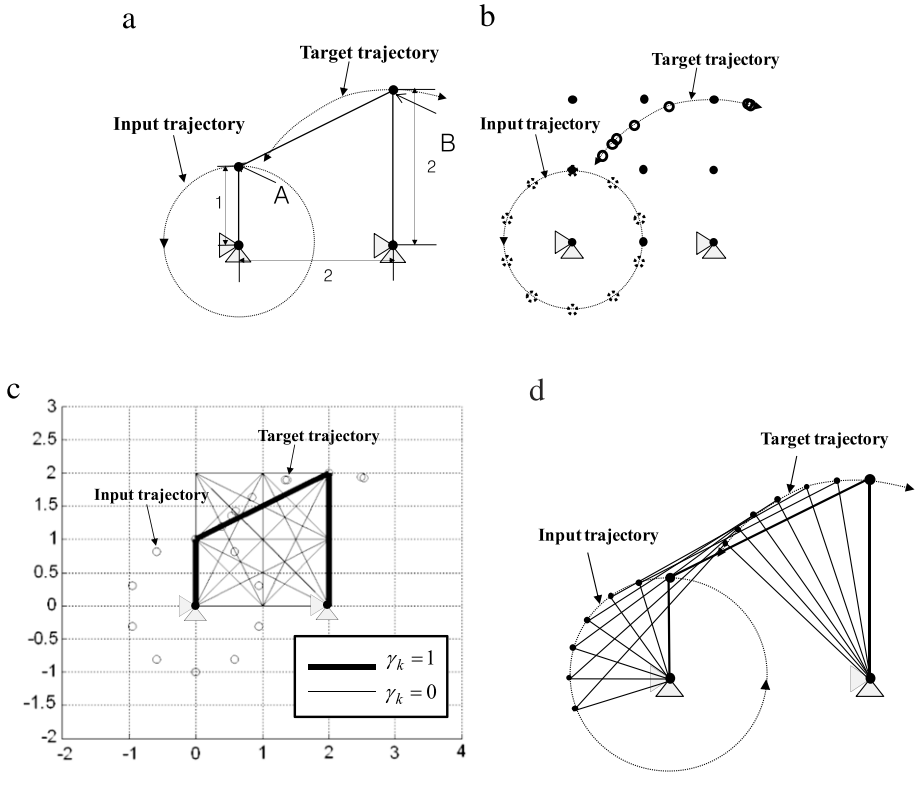

Fig. 13. Synthesis of the first four-bar mechanism. (a) A reference four-bar mechanism, (b) a distribution of nine masses, relative displacement inputs, and prescribed target displacements of the four-bar mechanism, (c) a design obtained through the developed optimization procedure, and (d) the actual movements of the design.

For this numerical correction step, the Lagrangian multipliers λ_k are unknown and determined. There are many numerical methods to calculate these Lagrangian multipliers. In this study, the heuristic SHAKE method is implemented. Note that the above

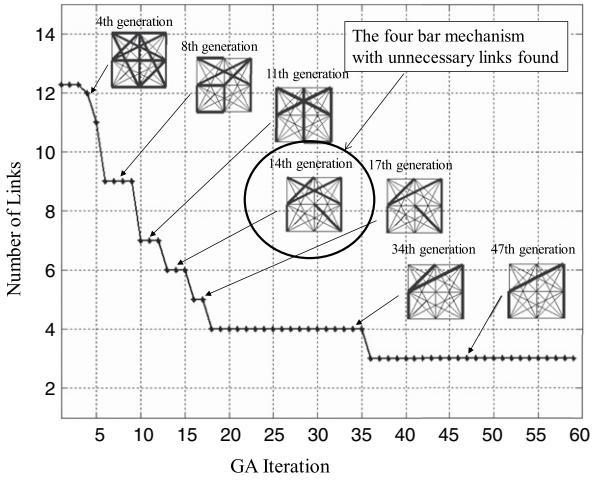

Fig. 14. Fitness curve and intermediate layouts.

simulation process is discrete with respect to time. Therefore, to obtain the detailed trajectory of a given mechanism, a fine time step, h, should be used.

In this update method, we modify (12) with a scalar ξ as follows:

$$\begin{aligned}\tilde{\tilde{\mathbf{r}}}_i(t+h) &= \tilde{\mathbf{r}}_i(t+h) - 2\frac{h^2}{m_i}\xi\mathbf{r}_{ij}(t),\\ \tilde{\tilde{\mathbf{r}}}_j(t+h) &= \tilde{\mathbf{r}}_j(t+h) + 2\frac{h^2}{m_i}\xi\mathbf{r}_{ij}(t).\end{aligned} \tag{13}$$

Here, $\tilde{\tilde{\mathbf{r}}}_i$ and $\tilde{\tilde{\mathbf{r}}}_j$ denote the uncorrected intermediate position vectors of the i-th and j-th masses, and ξ is an auxiliary constant replacing the Lagrangian multiplier. To discover the ξ value that satisfies the length constraint, the following conditions are re-derived; the updated positions with constant ξ should satisfy the length constraints.

$$\tilde{\mathbf{r}}_{ij}^2 = (\tilde{\mathbf{r}}_i - \tilde{\mathbf{r}}_j)^2, \qquad \tilde{\tilde{\mathbf{r}}}_{ij}^2 = (\tilde{\tilde{\mathbf{r}}}_i - \tilde{\tilde{\mathbf{r}}}_j)^2, \qquad \tilde{\tilde{\mathbf{r}}}_{ij}^2 = d_{ij}^2. \tag{14}$$

From the above conditions, it is possible to derive a second-order polynomial equation for ξ.

$$\left|\tilde{\mathbf{r}}_{ij} - 2h^2\left(\frac{1}{m_i} + \frac{1}{m_j}\right)\xi\mathbf{r}_{ij}\right|^2 = d_{ij}^2. \tag{15}$$

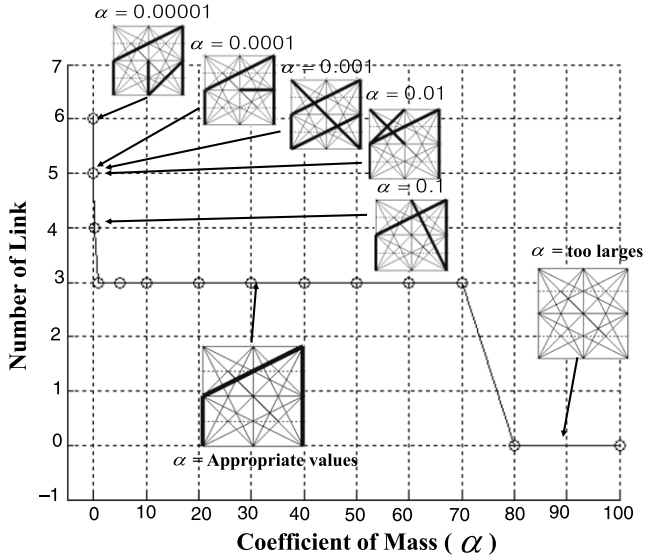

Fig. 16. Parameter effects of α in Eq. (21).

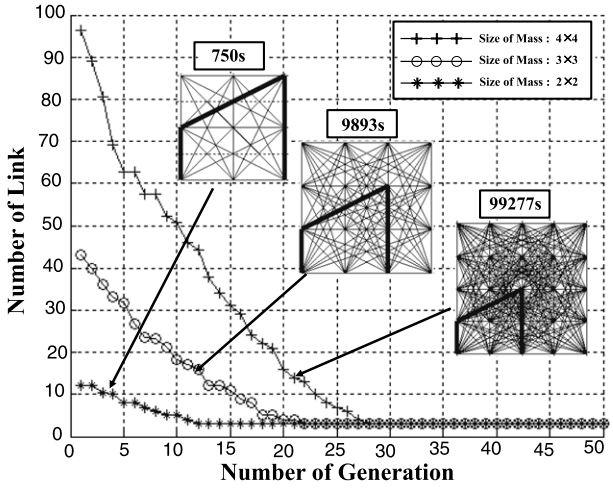

Fig. 17. The test of the optimization time for extended layouts.

One solution of (15) is as follows:

$$\xi = \frac{\tilde{\mathbf{r}}_{ij}^2 - d_{ij}^2}{4h^2\left(\frac{1}{m_i} + \frac{1}{m_j}\right)\tilde{\mathbf{r}}_{ij}\cdot\mathbf{r}_{ij}} = \underbrace{\frac{1}{4h^2\left(\frac{1}{m_i} + \frac{1}{m_j}\right)}}_{\text{A constant}}\frac{\tilde{\mathbf{r}}_{ij}^2 - d_{ij}^2}{\tilde{\mathbf{r}}_{ij}\cdot\mathbf{r}_{ij}}. \tag{16}$$

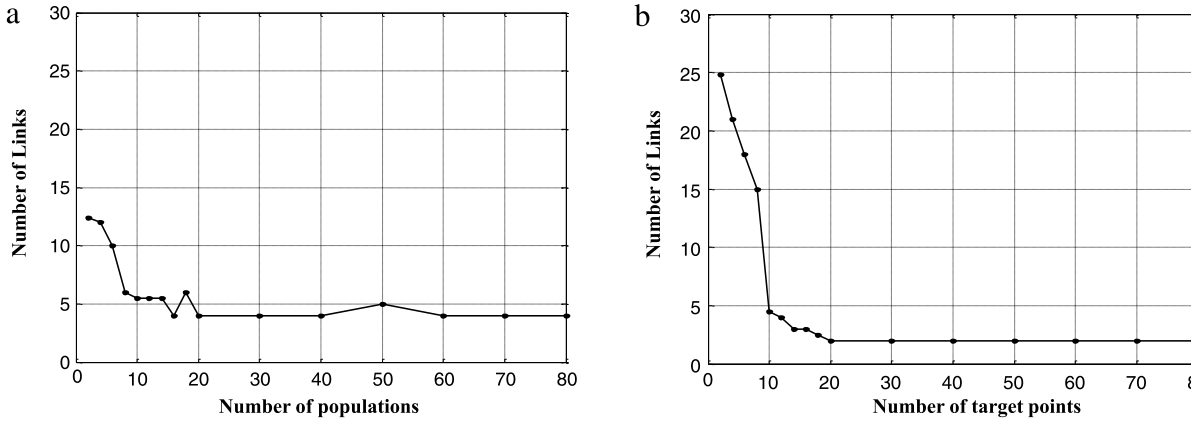

Fig. 15. Parameter effects on the number of links in the solution. The effects of (a) population numbers and (b) the number of input displacement points.

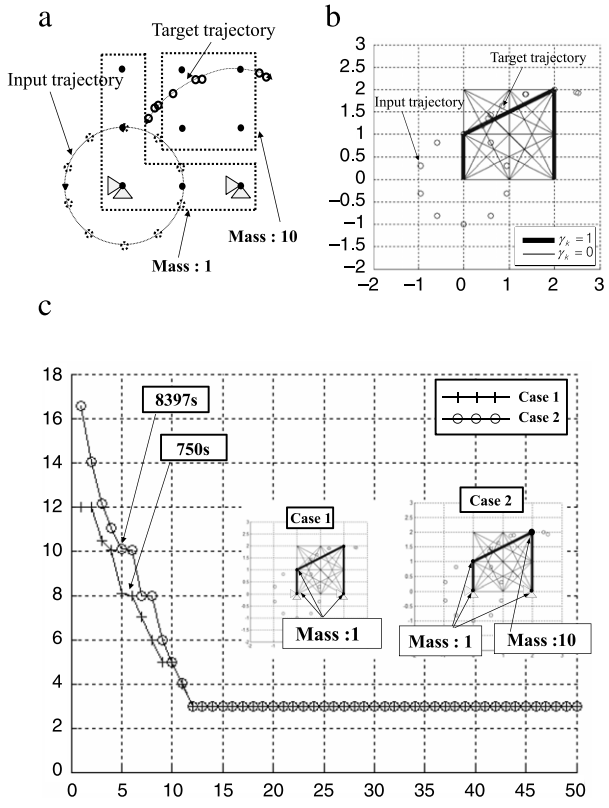

Fig. 18. The test of the different masses. (a) A test case with different mass values, (b) the obtained design and (c) the comparison.

As expected, even by updating the position vectors with a constant ξ, the length constraints are not satisfied because of the assumption in (13). Therefore, several iterations of (13)–(16) are in effect required. Furthermore, by simplifying the solution of ξ, the following iterations can alternatively be used for the heuristic update by replacing $\tilde{\mathbf{r}}_{ij}$ with r_{ij} and ignoring the constant in (16).

$$\tilde{\mathbf{r}}_i(t+h) = 2\mathbf{r}_i(t) - \mathbf{r}_i(t-h) + h^2\ddot{\mathbf{r}}_i(t) \tag{17}$$

$$\begin{aligned}\tilde{\tilde{\mathbf{r}}}_i(t+h) &= \tilde{\mathbf{r}}_i(t+h) - \xi\mathbf{r}_{ij}(t),\\ \tilde{\tilde{\mathbf{r}}}_j(t+h) &= \tilde{\mathbf{r}}_j(t+h) + \xi\mathbf{r}_{ij}(t)\end{aligned} \tag{18}$$

$$\xi = \frac{\mathbf{r}_{ij}^2 - d_{ij}^2}{4\mathbf{r}_{ij}^2}. \tag{19}$$

After several iterations of (17)–(19), the corrected positions $\tilde{\tilde{\mathbf{r}}}_i$ and $\tilde{\tilde{\mathbf{r}}}_j$ become identical to the solutions of (12). There are also similar approaches to add the rotation constraint among the unit masses. These methods can be applied to model arbitrary shape rigid links or constraint an angle between two rigid links. See [28] and the references therein for more details.

To illustrate the behavior of the SHAKE algorithm, Fig. 5 considers two mechanisms that are simple but sufficient to show the characteristics of the algorithm. The first is a standard four-bar mechanism, and the second has an additional rigid bar. Given this additional bar, the second mechanism clearly cannot move. Using the implemented SHAKE algorithm, we rotate the left rigid link 36°, simulate the motions of the remaining masses, and plot the calculated ξ in Fig. 5(c). Given that the locations of the masses in the first mechanism rotate without any problem, the ξ values of the three links converge to zero. In contrast, the ξ value of the additional bar of the second mechanism does not converge, indicating that this is a singular point. During the optimization process, when such non-convergences of ξ are observed, we halt the SHAKE algorithm and assign a very large value to the objective function (21) for the GA.

To check the accuracy of the kinetic analysis compared with the solution of the kinematic analysis, a simple four-bar mechanism analysis is performed in Fig. 6. To impose the rotation motion of the crank, the unit mass of the crank without the clamp condition is constrained to follow the trajectory of the crank; for the sake of illustration, six points equally divided are considered without loss of generality. As shown in Fig. 6 and Table 1, the solutions of the kinematic analysis are accurate. From an analysis point of view, the kinetic analysis is expensive but it can still be used as a basis of structural optimization for a rigid-body mechanism.

3. Binary topology optimization formulation for rigid-body mechanisms

This section aims to parameterize the existence of the constraint force and present an optimization formulation for the GA with integer design variables. The most state-of-the-art analytical approaches applicable to real mechanisms design feature workspace limitations, due in part to the fixed topology of the mechanism. Therefore, it would be convenient for a numerical

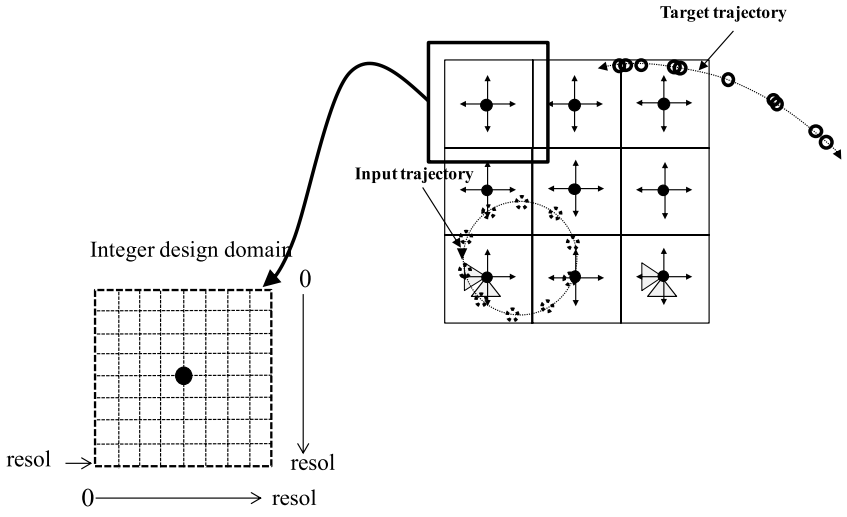

Fig. 19. The extension of the design variables.

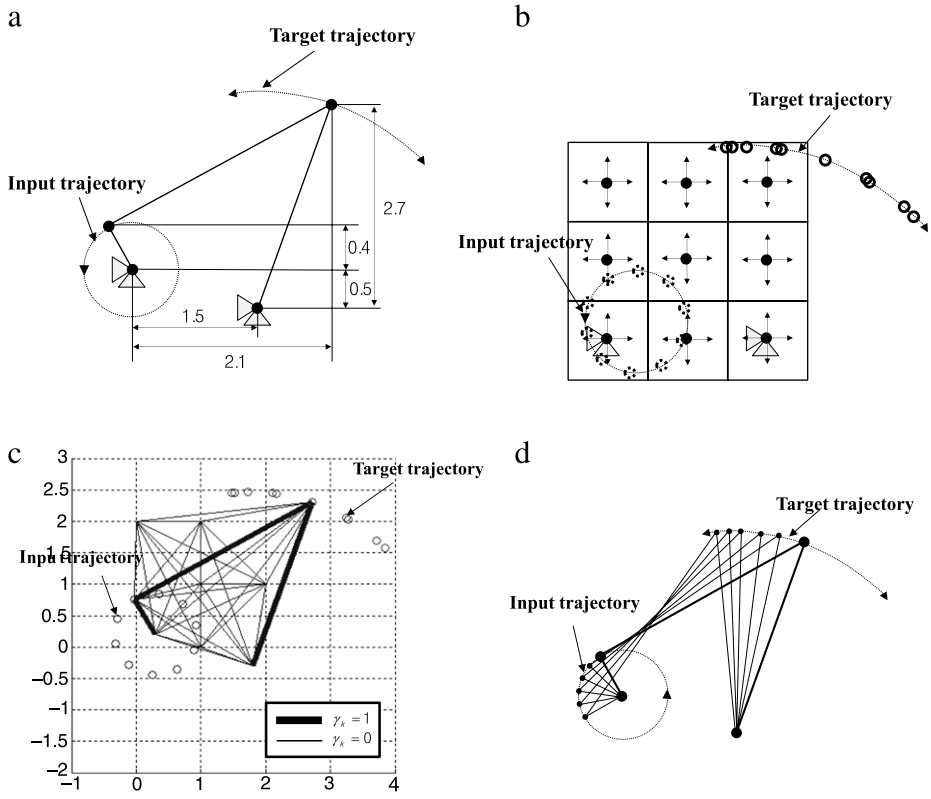

Fig. 20. Synthesis of the first four-bar mechanism with the location design variables (resol = 10). (a) A reference four-bar mechanism, (b) a distribution of nine masses, relative displacement inputs, and prescribed target displacements of the four-bar mechanism, (c) a design obtained through the developed optimization procedure, and (d) the actual movements of the design.

Table 1
The comparison between the kinematic and kinetic analyses of the four-bar mechanism.

Position	1	2	3	4	5	6
Kinematics	(2, 2)	(1.3659, 1.8968)	(0.8490, 1.6356)	(0.5352, 1.3617)	(0.3984, 1.1979)	(0.4, 1.2)
Kinetics	(2, 2)	(1.3659, 1.8968)	(0.8490, 1.6356)	(0.5351, 1.3617)	(0.3984, 1.1978)	(0.4, 1.2)

optimization algorithm to exploit and optimize the reachable workspace by changing the topologies of the mechanisms. To achieve this, the present study introduces integer design variables that determine the existence of the artificial length constraint forces among the masses in the SHAKE algorithm.

3.1. Parameterization of the existence of constraint forces

As stated in the preceding section, for the TO of rigid-body mechanisms, it is essential to devise a proper parameterization method for the existence of length constraint forces in (12). We find that we can assign one design variable to each link. By assigning a design variable with a value of 1 to the k-th design variable, the effective constraint forces for the k-th length constraint are applied to the corresponding masses. However, if the k-th design variable is assigned a value of 0, then the artificial constraint forces should disappear and the corresponding masses should move freely without any constraints. To implement this simple but effective feature numerically, we multiply the constraint force for the k-th link by the design variable γ_k. Note that because the values of ξ in (13) are different for each link, parameterization of the magnitude of the artificial constraint force as a standard density-based optimization is not allowed. For the feature above, we multiply the k-th length constraint in (18) by the design variable γ_k as follows (Fig. 7):

$$\begin{aligned}\tilde{\tilde{\mathbf{r}}}_i(t+h) &= \tilde{\mathbf{r}}_i(t+h) - \xi \mathbf{r}_{ij}(t)\gamma_k,\\ \tilde{\tilde{\mathbf{r}}}_j(t+h) &= \tilde{\mathbf{r}}_j(t+h) + \xi \mathbf{r}_{ij}(t)\gamma_k.\end{aligned} \tag{20}$$

This simple parameterization of the auxiliary constraint forces makes it possible to conduct TO of the rigid-body mechanism.

For an illustrative example of the realization of the rigid-body mechanism in the present parameterization method, let us consider the two rigid-body mechanisms in Fig. 8(a), (b). To model these mechanisms, nine equally spaced unit masses are distributed for the simulation of revolute joints. Without loss of generality, the masses are indexed from 1 to 9 in Fig. 8(c). In this configuration of indexed masses, 36 total connections or pairs are generated to simulate the rigid links. The links are also indexed as in the table of Fig. 8(c); given that the locations of the unit masses are fixed, there is a possibility that a rigid-body mechanism does not exist. This is a limitation of the present method. By assigning one design variable to each link, the total number of design variables becomes 36 ($9 \times 8/2$). After this assignment to represent the first four-bar mechanism (Fig. 8(c)), all design variables except γ_1, γ_{15} and γ_{35} are set to zero. In this configuration, for the second node moving along the prescribed input trajectory as a driver, the ninth mass precisely tracks the target trajectory of the first four-bar mechanism. For the second four-bar

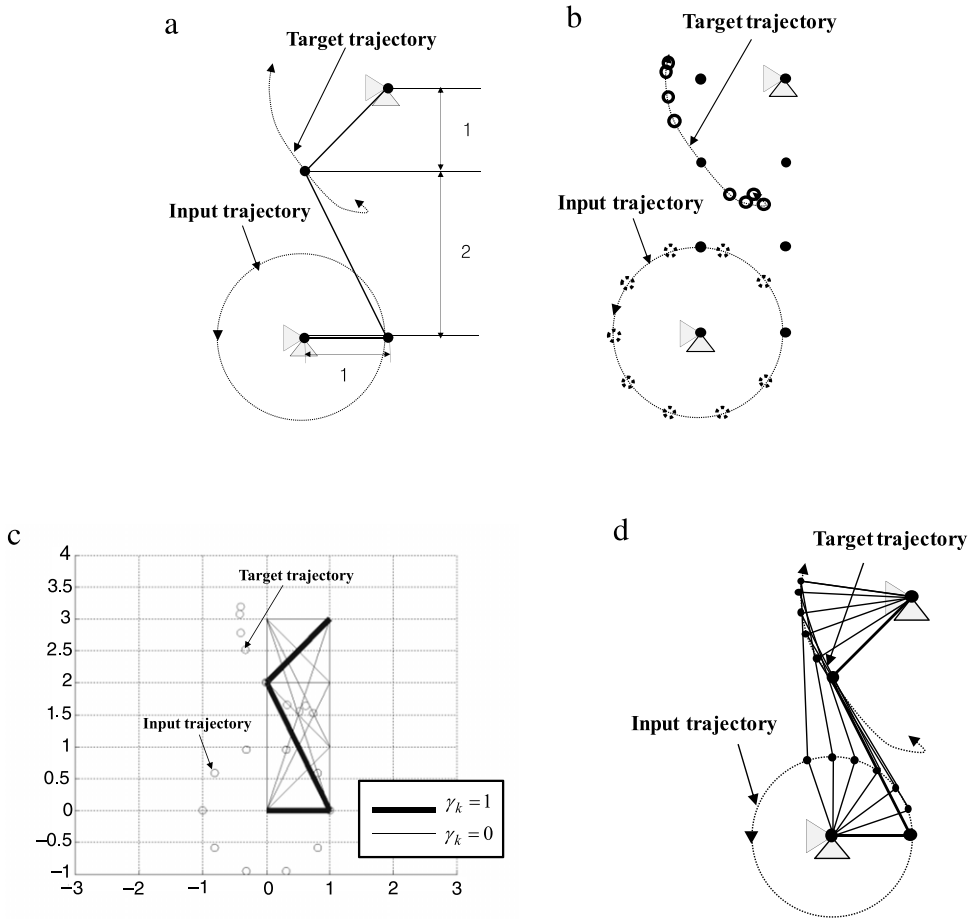

Fig. 21. Synthesis of the second four-bar mechanism. (a) A reference four-bar mechanism, (b) a distribution of eight masses, relative displacement inputs, and prescribed target displacements of the four-bar mechanism, (c) a design obtained through the developed optimization procedure, and (d) the actual movements of the design.

mechanism, all design variables except γ_2, γ_{21}, and γ_{35} are set to zero.

Although the above-mentioned parameterization method can describe arbitrary topologies, some limitations remain because of the initial mass distribution. In other words, because the position of each mass is determined by engineers or scientists before an optimization process, it may not be possible to discover an optimal topology for an arbitrary path trajectory as shown in Fig. 9. To overcome this limitation, we can develop an adaptive method to refine the positions of masses for future research topics. However, as the aim of this study is to demonstrate the validity of the concept for the first time, we concentrate on the validation of the present method as applied to path trajectories for which a distribution of masses exists.

3.2. Optimization formulation: GA

Given that the parameterization of the length constraint force uses binary design variables, a genetic algorithm (GA) mimicking the evolutionary process of nature may be one of the most suitable algorithms for the optimization problem of present concern [20]. The overall process of the simple GA used in this study is presented in Fig. 10.

To incorporate the GA into the optimization problem of interest, a fitness function must be devised. We note that in the process of discovering a rigid-body mechanism, we also seek to generate syntheses of planar rigid-body mechanisms with fewer rigid links at the same time. Thus, two objective functions are combined as follows[2]:

$$\Phi = \sum_{k=1}^{N_p} \left\| \mathbf{r}_W^k - \mathbf{r}_{W,\text{Target}}^k \right\| + \alpha \sum_{k=}^{N} \gamma_k, \tag{21}$$

where the k-th calculated trajectory of a work point of a given design and the k-th target trajectory of the work point are denoted by $\mathbf{r}_W^k$ and $\mathbf{r}_{W,\text{trajectory}}^k$, respectively; as we only consider the displacements of unit masses, the speeds of the unit masses can be chosen arbitrarily. The number of work points and the number of design variables are denoted by N_p and N, respectively. The first term of (21) measures the differences between the path of the work point and the target trajectory as shown in Fig. 11(a). Furthermore, to minimize the usage of links, a second term with a scaling factor of α is added. Without the second term, rigid-body mechanisms with unnecessary branches are obtained as shown in Fig. 11(b).

3.3. An extension to design support

The developed optimization approach also can be extended to identify the optimal locations of clamp boundary conditions. For

[2] Although alternatively to the object in (21), we can consider the actual length of links as follows. Alternative Object: $\Phi = \sum_{k=1}^{N_p} \left\| \mathbf{r}_W^k - \mathbf{r}_{W,\text{Target}}^k \right\| + \alpha \sum_{k=}^{N} \gamma_k l_k$ (where l_k is the length of the k-th link).

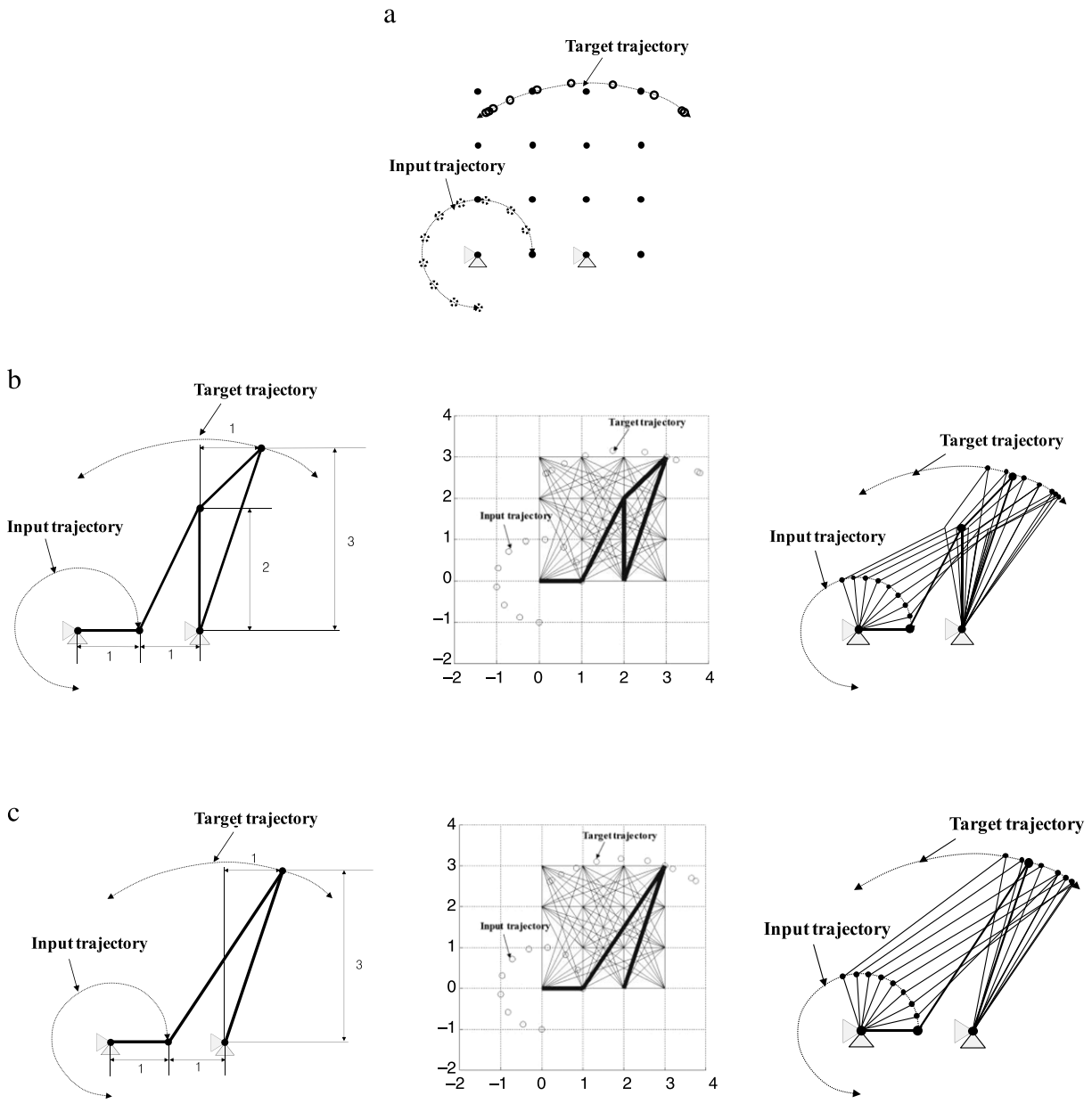

Fig. 22. Local optima issue. (a) A given trajectory, (b) an obtained local optimum, and (c) a second local optimum.

this purpose, a design variable vector is added to the existing design variable vector as follows:

$$\boldsymbol{\gamma} = [\underbrace{\gamma_1 \cdots \gamma_N}_{\text{Link}}, \underbrace{\gamma_{N+1} \cdots \gamma_{N+M}}_{\text{Boundary condition}}], \tag{22}$$

where γ_1 to γ_N are the design variables determining the existence of each rigid link and γ_{N+1} to γ_{N+M} are the design variables determining the clamp condition. The number of masses is denoted by M. For illustrative purposes, consider the example in Fig. 12. As shown in Fig. 12(a), by assigning 1 to γ_{N+1} and γ_{N+9}, the two masses are clamped; hence, they can be considered as clamped revolute joints. On the other hand, by setting γ_{N+9} to zero, this clamped condition can be removed as shown in Fig. 12(b). Thus, by optimizing these additional design variables, it is possible to identify optimal clamp conditions while designing the mechanism. An extension to clamp one direction displacement can also be considered without loss of generality.

4. Synthesis of two-dimensional rigid-link mechanisms

To validate the usefulness and performance of the developed theory and numerical method in the preceding sections, the TO of several syntheses of two-dimensional rigid-body mechanisms are considered.

Example 1 (*Synthesis of Four-bar Mechanism System*)**.** *Four-bar mechanism* 1.

For the first numerical example, the simple four-bar link mechanism shown in Fig. 13 is considered. Despite its simple geometry, this mechanism can demonstrate the potential of the developed optimization procedure for mechanism design. To calculate the reference input and output trajectory points, the revolute joint marked by (A) is first rotated counter-clockwise and the trajectory points of joint (B) are recorded as shown. For a numerical test, the ten marked points of work point B are

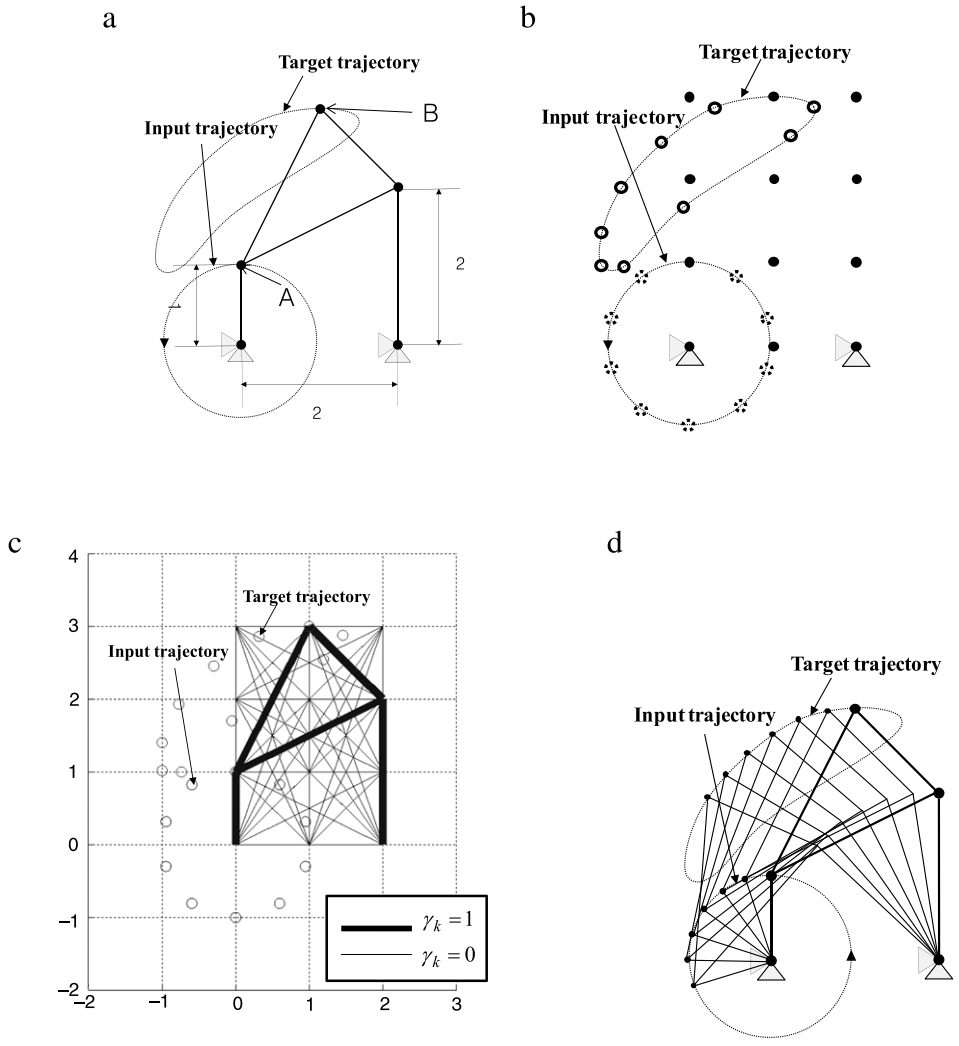

Fig. 23. Synthesis of a four-bar mechanism with a triangular body. (a) A reference four-bar mechanism, (b) a distribution of 12 masses, relative displacement inputs, and prescribed target displacements of the four-bar mechanism, (c) a design obtained through the developed optimization procedure, and (d) the actual movements of the design.

established as the target points. For TO, nine unit masses are uniformly distributed and the degrees of freedom of the bottom two corner nodes are clamped. The total number of possible links connecting these masses is 36; indeed a 36-bit array is generated for the design variables. By applying the developed optimization procedure, the four-bar mechanism in (c) can be obtained after 60 GA iterations. As shown in the figure, it is possible to obtain the rigid-body mechanism successfully.

Fig. 14 shows the fitness curve and the intermediate layouts during GA iterations. At around the 15th iteration, a design that precisely tracks the target trajectory can be found with extra branches or links. The remaining GA iterations remove these unnecessary branches. As illustrated, the developed approach can effectively discover the four-bar mechanism.

Fig. 15 shows the effects of the number of target trajectory points in (21) and the population number in discovering the optimal layout on the number of links. We can interpret the convergence of the number of links to 4 as the convergence of the GA populations to the solution. From this figure, it appears that the increase in the number of target points accelerates the convergence of the GA populations to the solution, although it takes considerable computation time per GA iteration. We also test the effect of population number, as shown in Fig. 15(b). As is observed in other types of problem, increasing the number of populations leads to better solutions in the GA framework. Because the scaled sum of the number of links is added to the norm of the distance differences in (21), the present optimization algorithm is influenced by the choice of α. With a relatively large value, it does converge to the zero-link mechanism, whereas, with a relatively small value, some extra branches remain, as shown in Fig. 16. Thus, some executions of trial by error should be conducted to define a range of this value. Based on our numerical tests, a range about one to several tens of the distance norm is acceptable. Also because the present optimization algorithm is based on the genetic algorithm, the computation time is increased by the number of the design variables. To test this feature, we extend the design domain of the Fig. 13 in Fig. 17. As shown, by extending the design domain, the numbers of the design variables are increasing exponentially. As a result, the optimization time as well as the solution time is increased, as shown in Fig. 17.

Effect of mass.

Until now, unit masses have been employed for the four-bar mechanism design. To test the effect of the ratio of the masses on optimization, the above four-bar mechanism is re-solved with the different masses as in Fig. 18; the mass values of the four points are

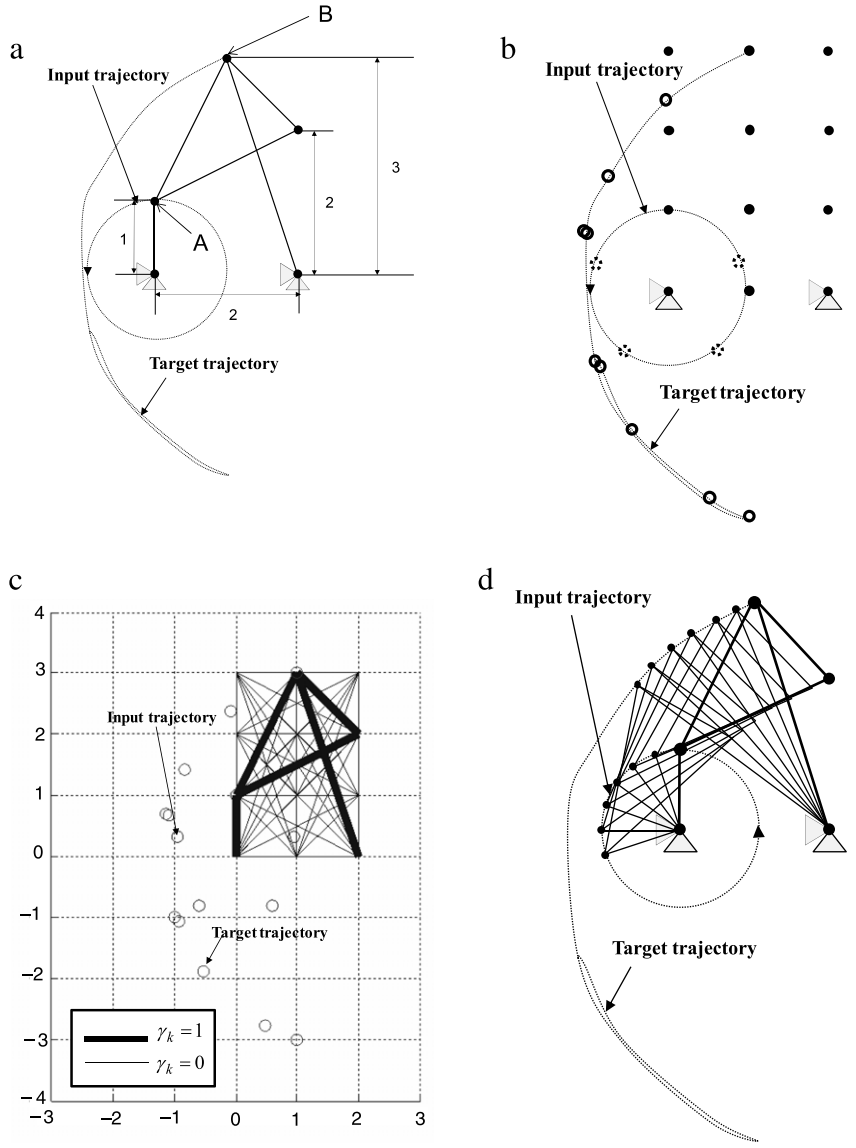

Fig. 24. Synthesis of a second four-bar mechanism with a triangular body. (a) A reference four-bar mechanism, (b) a distribution of 12 masses, relative displacement inputs, and prescribed target displacements of the four-bar mechanism, (c) a design obtained through the developed optimization procedure, and (d) the actual movements of the design.

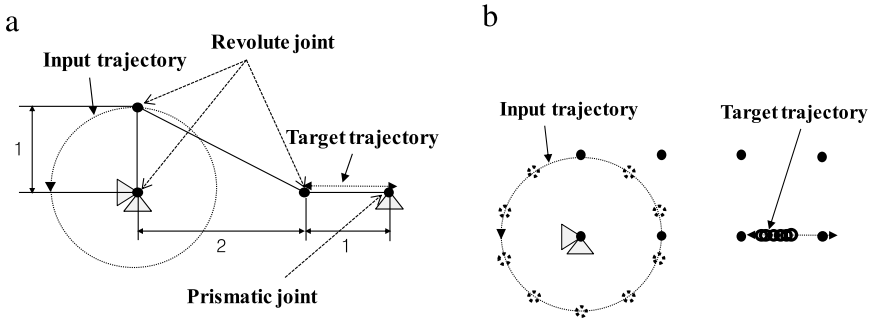

Fig. 25. Slider–crank mechanism. (a) A reference four-bar mechanism, and (b) a distribution of eight masses, relative displacement inputs, and prescribed target displacements of the four-bar mechanism.

set to 10. It turns out that the change of the masses of the four-bar mechanism does affect the SHAKE algorithm. Because the heavier mass moves slowly, the iteration number of the SHAKE algorithm becomes large. Nevertheless, the resulting trajectory is the same. Therefore, the same result can be obtained. Fig. 18 compares the design iterations of each case.

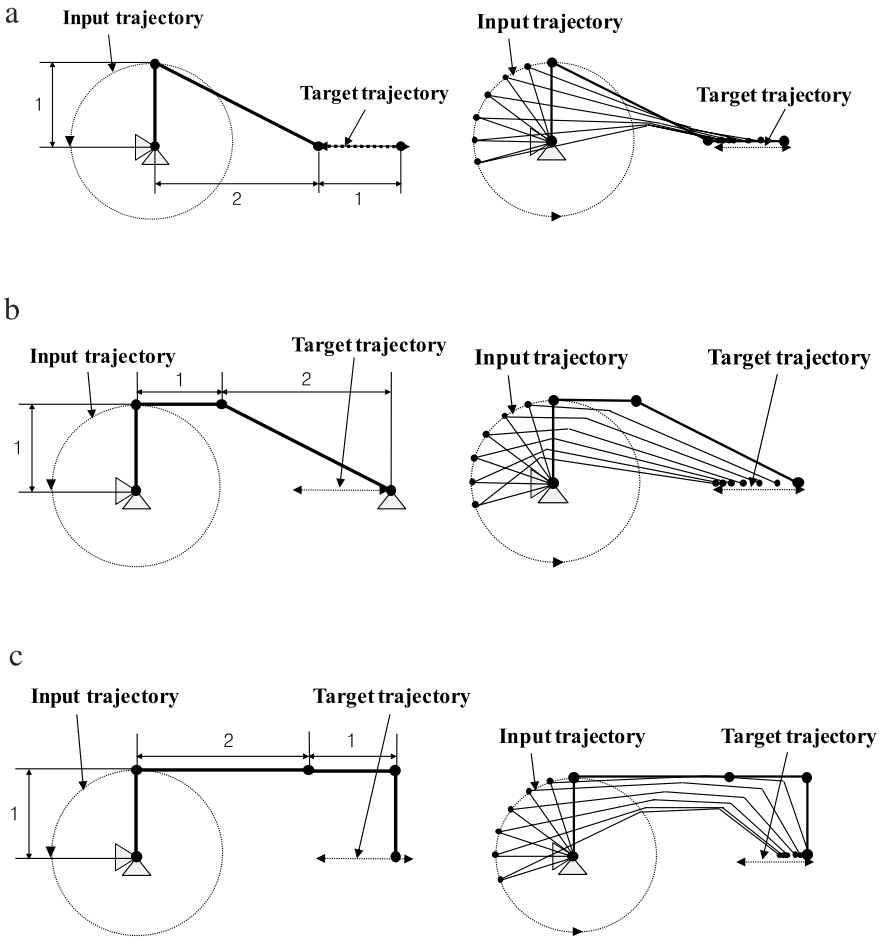

Fig. 26. Obtained designs for the slider–crank mechanism.

Parameterization of the locations of the unit masses.

As stated in Fig. 9, the initial distribution of the unit masses is important in terms of the optimization and there is a high possibility not to obtain the mechanism. To overcome this limitation, it is possible to parameterize the locations of the unit masses as follows:

$$\boldsymbol{\gamma} = [\underbrace{\gamma_1 \cdots \gamma_N}_{\text{Link}}, \underbrace{\gamma_{N+1} \cdots \gamma_{N+M\times 2}}_{\text{Location variables}}] \tag{23}$$

$$\begin{aligned} &\gamma_i \in [0, 1] \quad \text{when } 1 \le \gamma_i \le N \\ &\gamma_i \in [1, \text{resol}] \quad \text{when } N+1 \le \gamma_i \le N + M \times 2, \end{aligned} \tag{24}$$

where γ_1 to γ_N are the design variables determining the existence of each rigid link and γ_{N+1} to $\gamma_{N+M\times 2}$ are the design variables determining the locations of the masses. The number of masses is denoted by M. The resolution of the locations is denoted by "resol" in (24) in Fig. 19. With the above formulation, the unit masses can move inside the small rectangular boxes around each mass with equal "resol" abscissa.

To test this extension, the rigid-body mechanism in Fig. 20(a), which is a modified four-bar mechanism, is considered as a reference mechanism and evenly distributed masses are considered in Fig. 20(b). To find this mechanism, the movements of the masses are parameterized as in (24). Fig. 20(c) shows the obtained design which is exactly the same as the design of Fig. 20(a).

Four-bar mechanism 2.

As a second optimization example, we consider the synthesis of another four-bar mechanism, shown in Fig. 21. Compared with the trajectory of the first four-bar mechanism, we observe a relatively complex trajectory. The initial mass distributions and target trajectory points used for the GA are presented in Fig. 21(b). As in the first example, dozens of iterations result in the optimal rigid-body design shown in Fig. 21(c).

Local optima issue.

From several numerical tests, it is also possible to show that the developed approach can identify many local optima simultaneously using the advantages of multiple GA populations. In contrast, only a single local optimum can be found in the conventional TO theory based on a gradient-based optimizer; this feature is regarded as its shortcoming. However, using the GA framework, we can circumvent the local optima issue effectively with the help of multiple populations. For example, we solve the mechanism design problem of providing the target trajectory using the input trajectory shown in Fig. 22(a), which is actually obtained from the design of Fig. 22(b). After solving this optimization problem with the newly developed approach, we obtain the two solutions in Fig. 22(b) and (c). The target trajectory of the two solutions precisely matches the target trajectory in (a), although the layouts are different. In conclusion, it appears that we can readily discover multiple solutions because of the peculiar solution search characteristics of the GA.

Example 2 (*Synthesis of Four-bar Link System with an Additional Body*)**.** To consider the synthesis of a more complex mechanism, syntheses of mechanisms with a triangular body are shown in Figs. 23 and 24. Unlike the previous two examples, the optimization algorithm must discover the upper triangular geometries as

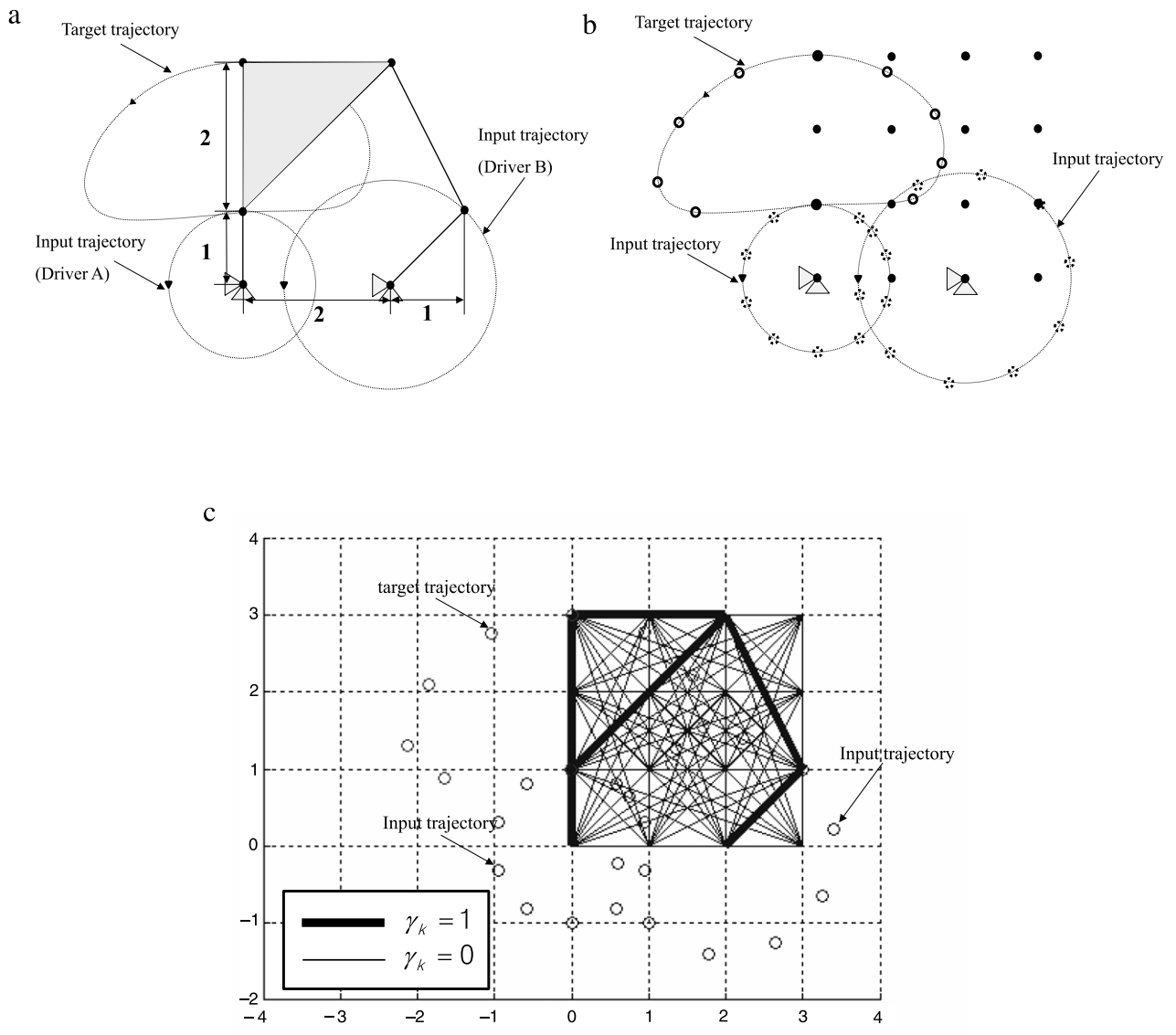

Fig. 27. Five-bar mechanism. (a) A reference five-bar mechanism, (b) a distribution of 16 masses, relative displacement inputs, and prescribed target displacements of the five-bar mechanism and (c) an optimized layout.

well as the four-bar mechanisms. As in the first example, the drivers marked by A are rotated and the trajectories marked by B are established as the target trajectories (Figs. 23(a) and 24(a)). After several hundred evolutions, the designs in Figs. 23(c) and 24(c) are obtained.

Example 3 (*Synthesis of Four-bar Link System with Prismatic and Revolute Joints*)**.** To show the versatility of the developed algorithm, a slider–crank mechanism with prismatic and revolute joints is considered for the third numerical example (Fig. 25). To solve this optimization problem, eight masses are distributed in total. With the developed optimization procedure, the three designs shown in Fig. 26 are obtained. As noted in the first numerical example, multiple optimization results can be found as global optima.

Example 4 (*Synthesis of Five-bar Mechanisms (Two Degrees Mechanism)*)**.** By applying the present optimization algorithm, it is also possible to synthesize complex mechanisms. To show this feature, the five-bar mechanism with two degrees of freedom in Fig. 27 is considered. Depending on the locations of the drivers, different trajectories can be obtained. To find this mechanism, the configuration of Fig. 27(a) is chosen as a reference mechanism. By applying the developed approach, the optimum solution in Fig. 27(c) generating the trajectory of Fig. 27(b) is found. This example shows that the present optimization algorithm can solve mechanism synthesis problems with multiple degrees of freedom.

Example 5 (*Synthesis of a Sine Curve Generation Mechanism*)**.** As another four-bar example, this example considers the synthesis of a sine curve generation mechanism as shown in Fig. 28(a). As in the previous example, one left link is chosen as the crank and an optimal layout generating the subsection of the sine curve shown in Fig. 28(b) is the pursuit. As shown, using the present approach, it is possible to find a design generating the sine curve in Fig. 28(b) and (c).

Example 6 (*Synthesis of a Peaucellier–Lipkin Linkage Mechanism*)**.** To show the validity of the present algorithm, the Peaucellier mechanism shown in Fig. 29(a) is set as a reference design. This mechanism is known as one of the popular mechanisms transforming rotational motion into perfect straight line motion. As shown in Fig. 29, the present algorithm can find this Peaucellier–Lipkin linkage successfully without any difficulty.

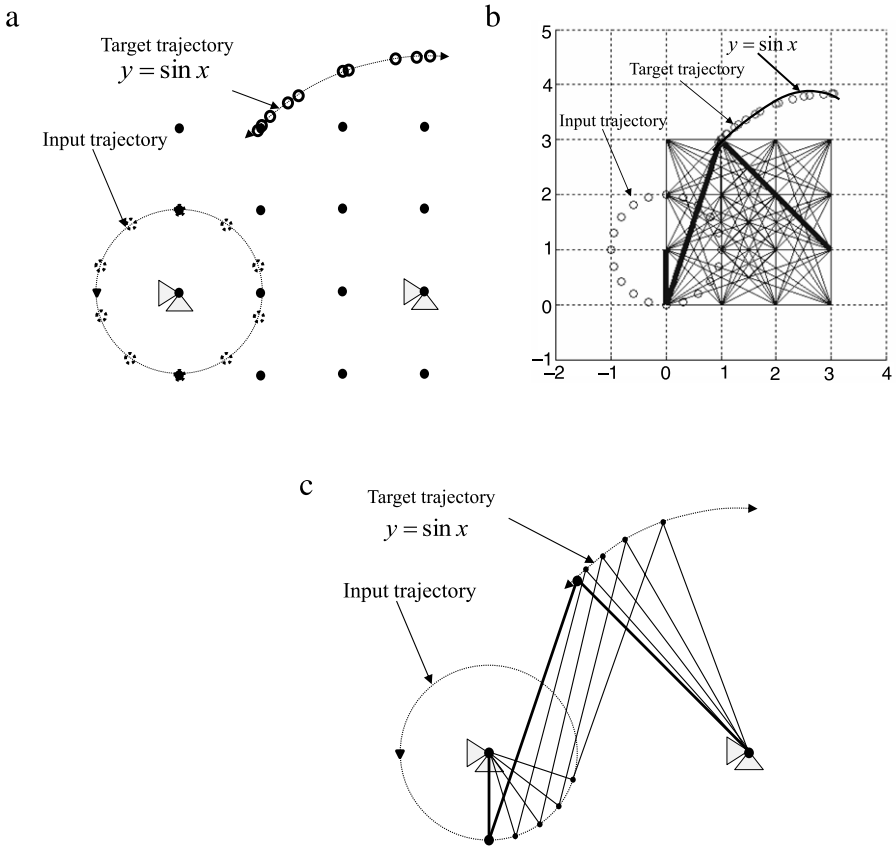

Fig. 28. Sine curve generation mechanism. (a) A distribution of 16 masses, relative displacement inputs, and prescribed target displacements, (b) an optimized layout and (c) the movement of the design.

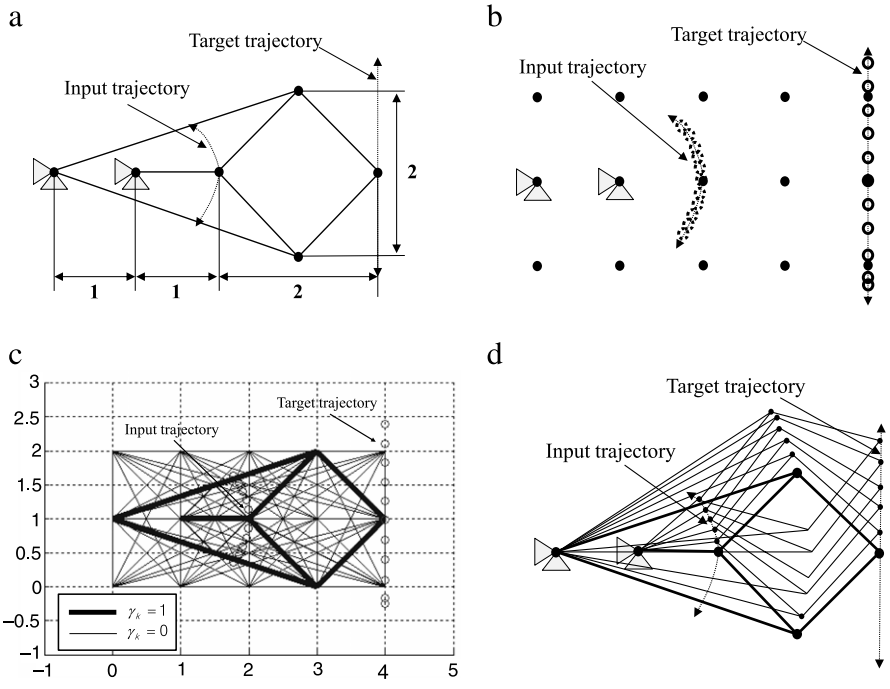

Fig. 29. Peaucellier–Lipkin mechanism. (a) A reference Peaucellier–Lipkin mechanism, (b) a distribution of 15 masses, relative displacement inputs, and prescribed target displacements, (c) an optimized layout and (d) the movement of the obtained design.

Example 7 (*Synthesis of a Complex Linkage Mechanism*)**.** To show the local optima characteristic of the present algorithm, the complex linkage mechanism in Fig. 30 is considered. The objective of the linkage mechanism is to transform the rotational motion into

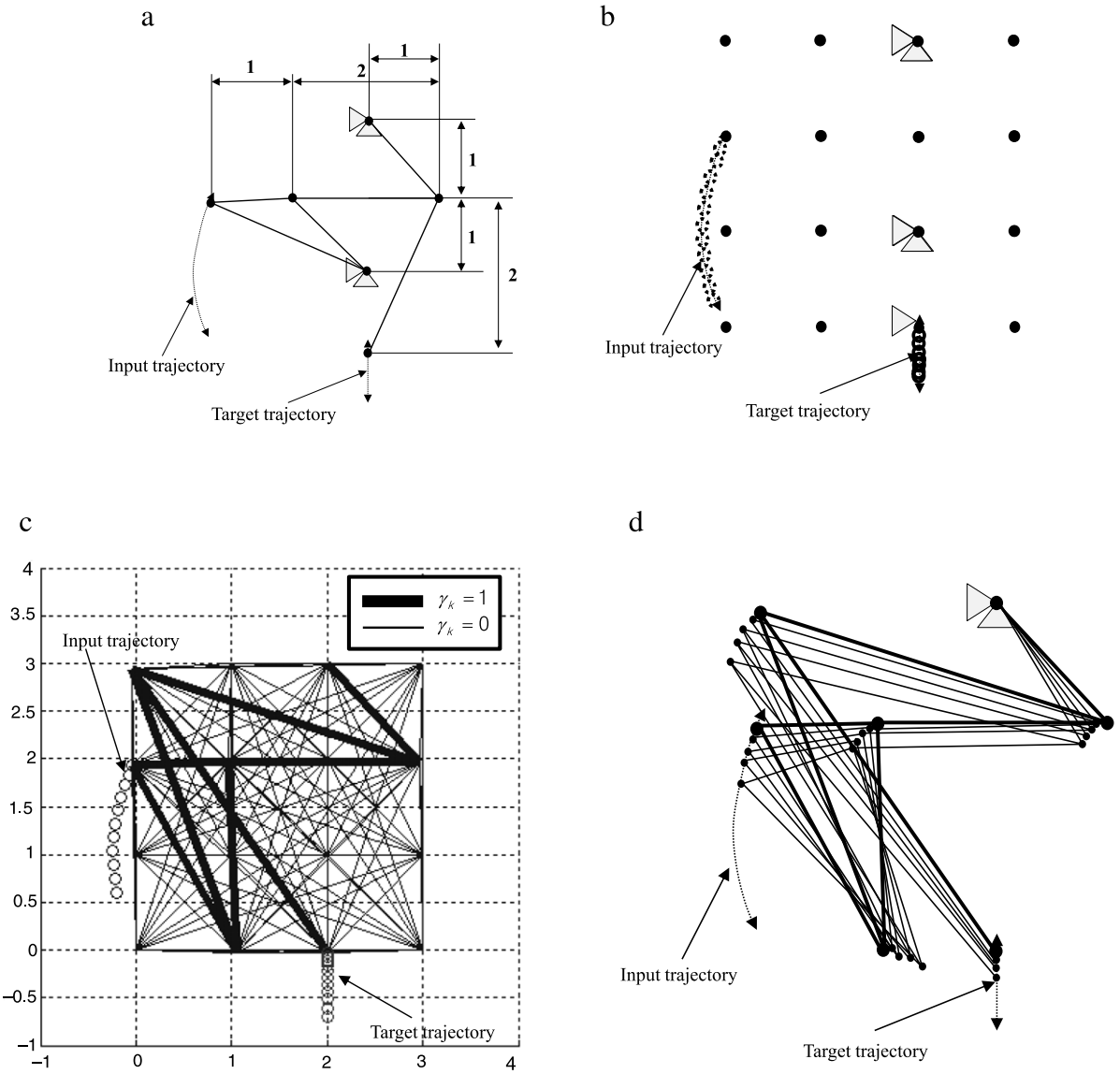

Fig. 30. A complex linkage mechanism. (a) A reference linkage mechanism, (b) a distribution of 16 masses, relative displacement inputs, and prescribed target displacements, (c) an optimized layout and (d) the movement of the design.

up and down straight motion. To solve this optimization problem, the movements of the reference linkage mechanism in Fig. 30(a) are analyzed and are set as the input trajectory and the target trajectory in the optimization process. Fig. 30(b) and (c) show the used distribution of the unit masses and the obtained mechanism which is different to (a) but follows the exact trajectory. As explained in Example 1, the present algorithm can find another local optimum mechanism easily.

Furthermore, it is recognized that many local optima can exist by allowing the design of the boundary condition.[3] To test this feature, the same trajectory problem is solved by allowing the boundary design. Here, the design variables are extended as

$$\boldsymbol{\gamma} = [\underbrace{\gamma_1 \cdots \gamma_N}_{\text{Link}}, \underbrace{\gamma_{N+1} \cdots \gamma_{N+M}}_{\text{Boundary condition}}], \tag{25}$$

where the number of design variables for the existences of the artificial forces is $N(=120)$ and the number of design variables parameterizing the type of the boundary condition is $M(=32)$. Fig. 31 shows the optimized layout. Here, it is noticed that the location of the sliding boundary condition at the working point is designed and that different clamp conditions are found.

Example 8 (*Design Boundary Condition and Rigid Link*)**.** As mentioned already, the developed optimization algorithm can be easily extended to design supports of rigid-body mechanisms by considering additional design variables in (22). To demonstrate this feature *specifically*, a target mechanism with five used links is considered in Fig. 32(a). The bottom left and bottom right joints are clamped. The motion of the top right joint is recorded as the target trajectory. To discover this mechanism, 20 masses in total are distributed in Fig. 32(b). Here, we set up the optimization problem with only the bottom left mass clamped, as shown in Fig. 32(b). Therefore, the optimization algorithm must find the other clamp condition as well as the distribution of rigid links. In this numerical example, the total number of links defined among the 20 masses and the number of additional design variables for the clamp condition are 190 and 19, respectively; hence, the number

[3] This was recommended by an anonymous reviewer.

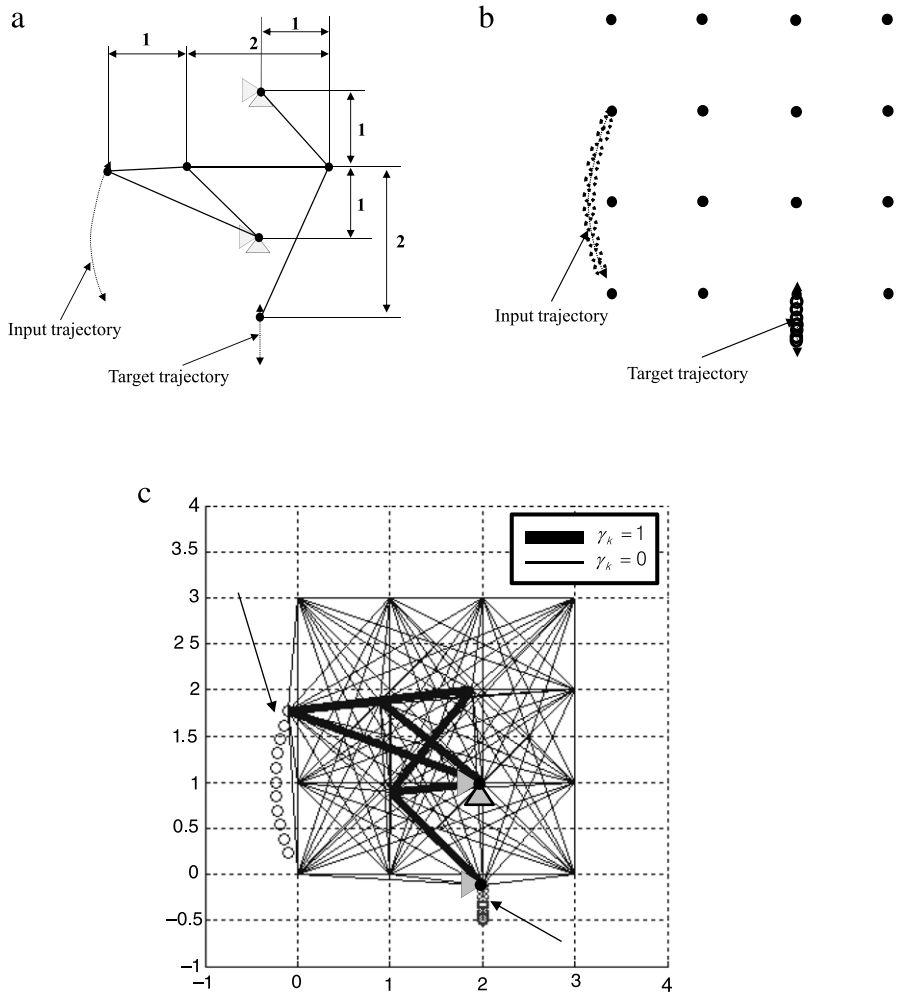

Fig. 31. A new linkage mechanism by additionally optimizing the boundary condition. (a) A reference linkage mechanism, (b) a distribution of 16 masses, the relative displacement inputs, and the prescribed target displacements, and (c) a new optimized layout.

of design variables is 209. Using the developed algorithm with the additional design variables, we can successfully discover the three global optima in Fig. 32(c), whose trajectories precisely match the prescribed target trajectory. As shown in the figure, the total number of links is 5 for both of the two designs whereas the number of the links of the last design is 4. Not surprisingly, the first design is same as the design in Fig. 32(a). However, the second and third may be difficult to discover through the intuition of an engineer. It seems that the considered mechanism synthesis problem lacks convexity. This numerical example in particular reveals that the additional parameterizations of the locations of the unit masses and the boundary condition make the convexity issue serious. From a mathematical point of view the present optimization problem has a lot of local optima and the present constraint force deign method with a GA finds one of them.

5. Conclusions

In this paper, we present a new design method, called the force constraint design method, as an alternative to existing mechanism synthesis methods in generating rigid-body mechanisms for output path generation. Although the size optimization of joint positions and lengths of links of a fixed topology mechanism synthesis is well studied, the black box approach finding an optimal connection for rigid-body mechanism has seldom been studied. To contribute to this research field, some new research is proposed and presented in this paper. We perform kinetic rather than kinematic analyses of the positions of revolute joints or work points of rigid-body mechanisms to allow topology optimization of rigid-body mechanism; strictly speaking, the employed simulation approach indirectly calculates the motions of rigid-body mechanism through kinetic analysis. This is one of the key ideas presented in this paper. With this present procedure, it is possible to find the optimal configurations of the rigid links as well as the optimal support conditions. A limitations is that the initial mass distribution limits the design space of the rigid links; this is one of our future research topics. Unit masses are used to represent joints or work points. The Lagrangian multiplier method, which has already been developed for robot simulation, DNA simulation, molecular dynamics, etc., is employed to present rigid links and constraints among joints and work points. For topology optimization, binary design variables with values of zero or one are assigned to auxiliary pair forces between two masses. By determining the binary design variables that minimize the gap between the target trajectory and a current trajectory of a given design, and minimizing the usage of links using a simple genetic algorithm, optimal rigid-body mechanisms are synthesized. To our knowledge, this kind of approach using the Lagrangian multiplier method and genetic algorithms has never been attempted previously. Given that simulations take little time and genetic algorithms do not require sensitivity analysis for the objective function, we can discover most optimal rigid-body mechanisms very quickly and robustly, at least for the

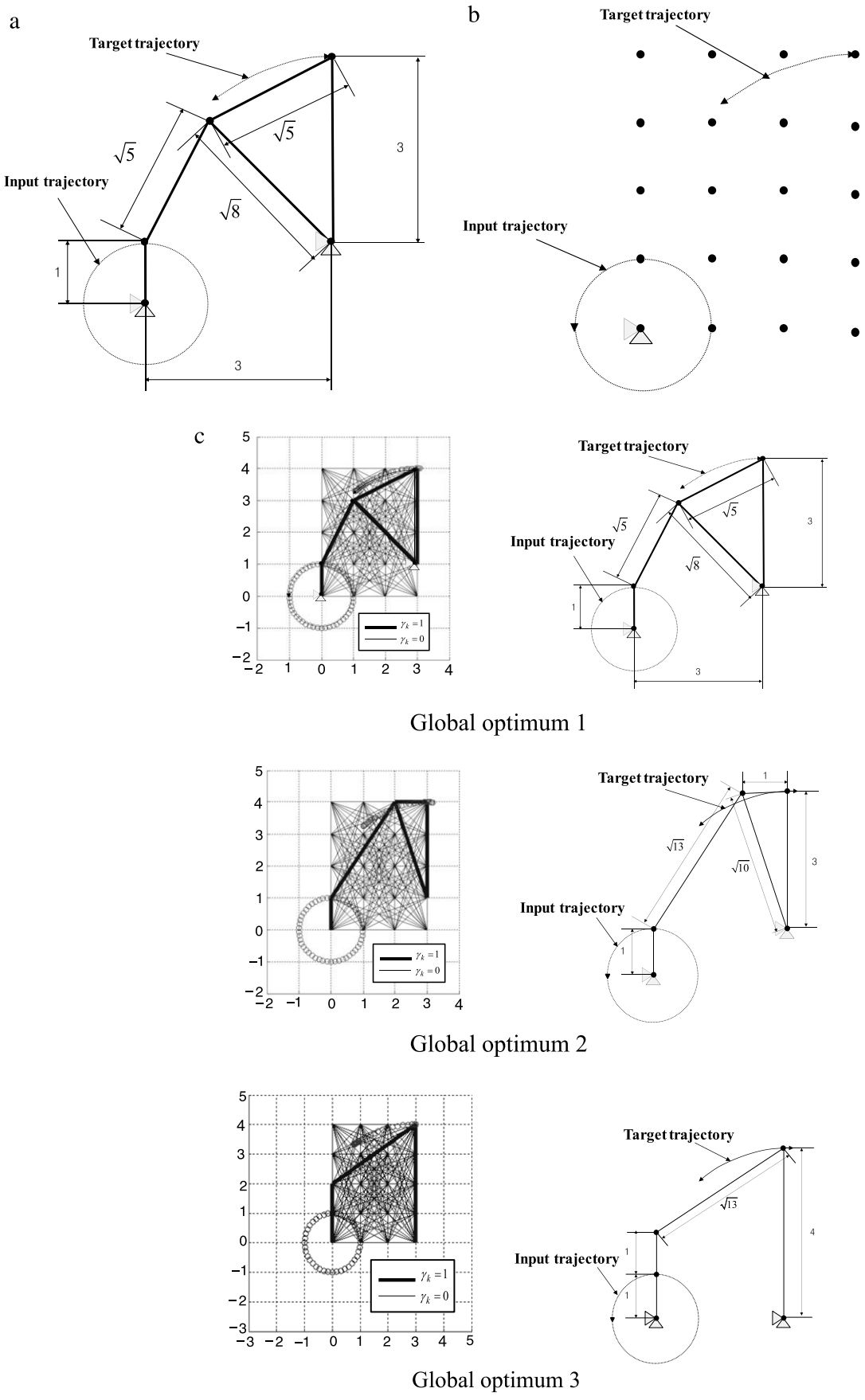

Fig. 32. Example of support design. (a) A target mechanism and trajectories, (b) the initial mass distribution, and (c) the three global optima obtained.

synthesis problems considered here. In a normal computational environment, it takes one or two hours for the four-bar mechanism problems and at most one day for the remaining problems.

However, the newly developed method has several limitations that require further study. Because this is our first attempt toward size, shape and topology optimizations of rigid-body mechanisms with the present constraint force design method, optimization examples that at least have optimal solutions have been considered. If there is no rigid-body mechanism with given target and input trajectories, the present approach has difficulties in finding the optimal rigid-body mechanism. In order to solve general optimization problems with arbitrary trajectories, other complex and real mechanism conditions such as the positions of linear or rotational actuators, the operation condition of actuators, and the types of link should be considered in the future. In addition, the existence of an optimum design for a general optimization problem with arbitrary trajectory should be studied in the future. Furthermore, it may be possible to develop mutation and crossover schemes suitable for the output path generation problem.

References

[1] Bendsøe MP, Sigmund O. Topology optimization: theory, methods and applications. New York: Springer-Verlag; 2003.
[2] Howell L. Synthesis of compliant mechanisms using continuum models in compliant mechanisms. John Wiley and Sons; 2001.
[3] Mankame N, Ananthasuresh GK. Topology synthesis of contact-aided-compliant mechanisms with small deformations. Computers and Structures 2004;82(15–16):1267–90.
[4] Yoon GH, Kim YY, Bendsøe MP, Sigmund O. Hinge-free topology optimization with embedded translation-invariant differentiable wavelet shrinkage. Structural and Multidisciplinary Optimization 2004;27(3):139–50.
[5] Bruns TE, Sigmund O. Toward the topology optimization of mechanisms that exhibit snap-through behavior. Computer Methods in Applied Mechanics and Engineering 2004;193(36–38):3973–4000.
[6] Prasad J, Diaz AR. Synthesis of bistable periodic structures using topology optimization and a genetic algorithm. Journal of Mechanical Design 2006;128(6):1298–306.
[7] Saxena A. Synthesis of compliant mechanisms for path generation using genetic algorithm. Journal of Mechanical Design 2005;127(4):745–52.
[8] Lu KJ, Kota S. Synthesis of shape morphing compliant mechanisms using a load path representation method. Smart Structures and Materials 2003;5049:337–48.
[9] Huang X, Xie YM. Topology optimization of nonlinear structures under displacement loading. Engineering Structures 2008;30(7):2057–68.
[10] Santer M, Pellegrino S. Compliant multistable structural elements. International Journal of Solids and Structures 2008;45(24):6190–204.
[11] Kamat MP, Ruangsingha P. Optimization of space trusses against instability using design sensitivity derivatives. Engineering Optimization 1985;8:177–88.
[12] Jang GW, Nam SJ, Kim YY. Sub-workspace design of binary manipulators using active and passive joints. Journal of Mechanical Science and Technology 2008;22(9):1707–15.
[13] Shean-Juinn C, Kota S. Automated conceptual design of mechanisms. Mechanism and Machine Theory 1999;34:467–95.
[14] Kawamoto A, Bendsøe MP, Sigmund O. Articulated mechanism design with a degree of freedom constraint. International Journal for Numerical Methods in Engineering 2004;61:1520–45.
[15] Kempe AB. On a general method of describing plane curves of the *n*th degree by linkwork. Proceedings of the London Mathematical Society 1876;7:213–6.
[16] Kempe AB. On conjugate four bar linkages. Proceedings of the London Mathematical Society 1878;9:133–47.
[17] Kim YY, Jang GW, Park JH, Hyun JS, Nam SJ. Automatic synthesis of a planar linkage mechanism with revolute joint by using spring-connected rigid block models. Journal of Mechanical Design 2007;129:930–40.
[18] Sedlaczek K, Gaugele T, Eberhard P. Topology optimized synthesis of planar kinematic rigid body mechanisms. Multibody Dynamics 2006;137(7):251–60.
[19] Wang MY. A kinetoelastic approach to continuum compliant mechanism optimization. In: ASME International Design Engineering Technical Conferences & Computers and Information in Engineering Conference. 2008.
[20] Holland JH. Genetic algorithms. Scientific American 1992.
[21] Kawamoto A. Path-generation of articulated mechanisms by shape and topology variations in non-linear truss representation. International Journal for Numerical Methods in Engineering 2005;64(12):1557–74.
[22] Youcef-toumi K. Analysis, design and control of direct-drive manipulators, Doctoral thesis, MIT, 1985.
[23] Tao J, Sadler JP. Constant speed control of a motor driven mechanism system. Mechanism and Machine Theory 1995;30(5):737–48.
[24] Neugebauer R, Drossel WG, Ihlenfeldt S, Harzbecker CH. Design method for machine tools with bionic inspired kinematics. CIRP Annals—Manufacturing Technology 2009;58(1):371–4.
[25] Zhang WJ, Li Q, Guo LS. Integrated design of mechanical structure and control algorithm for a programmable four-bar linkage. IEEE/ASME Transactions on Mechatronics 1999;4(4):354–62.
[26] Pennock GR, Israr A. Kinematic analysis and synthesis of an adjustable six-bar linkage. Mechanism and Machine Theory 2009;44(2):306–23.
[27] Aviles R, Vallejo J, Aguirrebeitia J, Bustos IFD, Ajuria G. Optimization of linkages for generalized rigid-body guidance synthesis based on finite element models. Finite Elements in Analysis and Design 2010;46(9):721–31.
[28] Hess B, Bekker H, Berendsen HJC, Fraaije JGEM. LINCS: a linear constraint solver for molecular simulations. Journal of Computational Chemistry 1997;18(12):1463–72.
[29] Krautler V, Wolfred F, Gunsteren V, Philippe H. Hunenberger, a fast SHAKE algorithm to solve distance constraint equations for small molecules in molecular dynamics simulations. Journal of Computational Chemistry 2001;22(5):501–8.
[30] van Gunsteren WF, Berendsen HJC. Algorithms for macromolecular dynamics and constraint dynamics. Molecular Physics 1977;34(5):1311–27.
[31] Forester RTimothy, William S. SHAKE, rattle and roll: efficient constraint algorithms for linked rigid bodies. Journal of Computational Chemistry 1998;19:102–11.
[32] Hocknet RW, Eastwood JW. Computer simulation using particles. New York: McGraw-Hill; 1981.
[33] Miyamoto S, Peter A. Kollman, settle: an analytical version of the SHAKE and RATTLE algorithm for rigid water models. Journal of Computational Chemistry 1992;13(8):952–62.
[34] Beeman D. Some multistep methods for use in molecular dynamics calculations. Journal of Computational Chemistry 1976;20(2):130–9.